Intuit Before Tuning: Type-1 and Type-2 Fuzzy Logic Controllers

Andriy Sarabakha[a], Changhong Fu[b], Erdal Kayacan[c,*]

[a]*School of Mechanical and Aerospace Engineering, Nanyang Technological University, 50 Nanyang Avenue, Singapore, 639798*
[b]*School of Mechanical Engineering, Tongji University, 4800 Caoan Road, Shanghai, 201804, China*
[c]*Aarhus University, Department of Engineering, DK-8000 Aarhus C, Denmark*

Abstract

Although a considerable amount of effort has been put in to show that fuzzy logic controllers have exceptional capabilities of dealing with uncertainty, there are still noteworthy concerns, e.g., the design of fuzzy logic controllers is an arduous task due to the lack of closed-form input-output relationships which is a limitation to interpretability of these controllers. The role of design parameters in fuzzy logic controllers, such as position, shape, and height of membership functions, is not straightforward. Motivated by the fact that the availability of an interpretable relationship from input to output will simplify the design procedure of fuzzy logic controllers, the main aims in this work are derive fuzzy mappings for both type-1 and interval type-2 fuzzy logic controllers, analyse them, and eventually benefit from such a nonlinear mapping to design fuzzy logic controllers. Thereafter, simulation and real-time experimental results support the presented theoretical findings.

Keywords: Type-1 fuzzy logic controllers, interval type-2 fuzzy logic controllers, fuzzy mapping, aerial robotics, unmanned aerial vehicles.

*Corresponding author
Email addresses: andriy001@e.ntu.edu.sg (Andriy Sarabakha), changhongfu@tongji.edu.cn (Changhong Fu), erdal@eng.au.dk (Erdal Kayacan)

1. Introduction

Nowadays, fuzzy logic controllers (FLCs) become one of the most popular model-free methods to control nonlinear systems when their precise mathematical model is challenging to obtain [1, 2]. Such popularity arises due to several characteristics of FLCs, e.g., to be able to improve both flexibility and robustness of the nonlinear system in the presence of disturbances or uncertainties by using the expert knowledge in the control design [3, 4]. For that reason, FLCs have been used for the control problems of mobile robots [5], in particular, as a more challenging control problem, unmanned aerial vehicles (UAVs) [6] whose precise mathematical model parameters are tedious to obtain.

Earlier FLCs were categorized as type-1 FLCs (T1-FLCs) and they are still the most widely used type of FLCs [6, 7]. There are several implementations of T1-FLC for the real-time applications [8, 9]. However, one of the main challenges in the design of T1-FLCs is the decision on the shape of membership functions (MFs) that are used [10]. In other words, there are no clear guidelines on how to choose the MFs and their corresponding parameters.

Recently, there has been a growing interest in a more advanced form of FLCs, namely type-2 FLCs (T2-FLCs) [11, 12]. The transition from T1-FLCs to T2-FLCs was justified by the fact that type-1 fuzzy sets (FSs) are able to deal effectively only with bounded levels of uncertainty, while real-world applications frequently have to deal with high levels and multiple sources of uncertainties [13, 14]. Better handling of the uncertainties, e.g., noisy measurements in the system, using T2-FLCs is provided by the additional degree of freedom benefiting from the footprint of uncertainty (FOU) in their FSs [15, 16]. However, the additional complexity arises from the inclusion of FOU as well as the third dimension [17]. Therefore, the research has tended to focus on interval T2-FLCs (IT2-FLCs) [18], rather than on general T2-FLCs [19], because the mathematical formulation of general T2-FLCs is much more complex than that of IT2-FLCs [20, 21]. The adoption of IT2-FLC allows reducing the computational complexity which is an immense benefit in real-time applications [22].

There are several types of control systems that use FLC as an essential system component. The majority of applications belong to the class of fuzzy proportional-integral-derivative (PID) controllers, where it is placed within the feedback control loop, and computes the PID actions through fuzzy inference [23]. In [24], more systematic analysis and design for conventional double-input T1-FLC (DI-T1-FLC) are presented. In [25], a fuzzy variable structure control is introduced for designing and tuning of DI-T1-FLC based on variable structure control theory. The fuzzy PID controller derived in [26] successfully demonstrated better performance than the conventional PID controller for many cases, particularly for nonlinear plants. In [27], a function-based evaluation approach is proposed for a systematic study of type-1 fuzzy PID controllers. In [28], a general technique is developed for rigorously deriving analytical input-output structure for fuzzy controllers that use Zadeh fuzzy AND-operator. In [29], an analytical structure for fuzzy PID controllers has been derived using L-type and G-type input FSs, trapezoidal output FSs, algebraic product triangular norm, bounded sum triangular co-norm, Mamdani minimum inference method and center of sums defuzzification method.

In recent studies, the impact of FOU on the single-input type-2 fuzzy mapping (FM) has been analysed [30]. Undoubtedly, an analytical expression of FM for IT2-FLCs provides an efficient tool to study IT2-FLCs [31]. Moreover, the modern computers can perform the basic algebraic operations, e.g., additions, subtractions, multiplication and divisions, much more efficiently than the operations of FSs, e.g., unions, intersections and implications, needed in fuzzy logic [32]. Therefore, the availability of an analytical form of FM will open new doors to the use of FLCs in real-time applications. Recently, FM for the single-input IT2-FLC case has been analytically derived in [33].

In [34], the analytical structure of a special class of IT2 fuzzy proportional-derivative (PD) and proportional-integral (PI) controllers that uses the Karnik-Mendel (KM) iterative algorithm for type-reduction has been presented. In [35], the mathematical input-output structure of Mamdani IT2 fuzzy PI controllers is derived for centroid and averaged defuzzifier. Instead of using common type-

reduction methods, IT2-FLC analysed in [35] approximates the type-reduced set by averaging embedded IT2-FLCs. In [36], some recent research results are summarized on understanding the fundamental differences between T1-FLCs and IT2-FLCs. It has been shown in [36] that IT2-FLC can implement a complex control surface that cannot be achieved by T1-FLC using the same rule-base. In [37], a technique is developed which is capable of deriving the analytical structure for a wide class of IT2-FLCs. In [38], an explicit solution is proposed to determine optimal switching points of KM method for double-input IT2-FLCs (DI-IT2-FLC). In [39], the analytical structural analysis of the simplest DI-IT2-FLC is presented. In [40], an approach to derive the analytical structure of a class of double-input Takagi-Sugeno FLCs is presented. Recently, in [41], the authors analysed the input-output relationship of various IT2-FLCs with trapezoidal FSs, and compared the difference in control performance via analytical structure approach. Nevertheless, an exhaustive analysis of FM for Mamdani DI-IT2-FLCs and real-time validation of the theoretical claims are still missing in the literature [42]. The continuity of T1-FLCs and IT2-FLCs have been introduced in [43]. Moreover, the study of other properties, such as symmetry and monotonicity, of FM of double-input FLCs is also missing in the literature.

In this study, by using some appealing observations, we have proposed an alternative systematic methodology to explicitly derive FMs for both DI-T1-FLC and DI-IT2-FLC. The proposed procedure to derive an analytical closed-form relationship between inputs and output provides information on the effect of FOU parameters. Moreover, the proposed methodology allows the generation of various control surfaces (CSs) by only reshaping the size of FOU. Furthermore, by only tuning one FOU parameter, it is possible to develop different controllers with less aggressive or more aggressive action. Additionally, the availability of FM allows reducing the computation time for FLCs drastically. In this work, T1-FLC and IT2-FLC with three triangular antecedent and three singleton consequent FSs are used to facilitate the illustration of the proposed method. Nevertheless, the presented method is not limited to a specific FLC and it can be applied to any T1-FLC or IT2-FLC to generate its FM in a

closed-form. In summary, the ultimate goal of this work is to contribute to the applicability of the double-input FLCs.

The main contributions of this work are:

- FMs for DI-T1-FLC and DI-IT2-FLC are analytically derived in closed-form with an alternative systematic approach;
- DI-IT2-FLC are analysed in terms of the role of their FOU parameters on the CS generation;
- the theoretical claims are validated in simulation and real-time for spacecraft and aerial robot control case studies.

This study is organised as follows. Section 2 revises the definition of T1-FLC and provides alternative derivation and mathematical analysis of its FM. In Section 3 the definitions, derivation and analysis are extended for IT2-FLC case. Sections 4 and 5 describes simulation and real-time case studies to confirm the theoretical assertions. Finally, Section 6 closes this work with conclusion and possible future work.

2. Double-Input Type-1 Fuzzy Logic Controller

First of all, some important definitions for T1-FLC are reviewed, which will allow to introduce DI-T1-FLC.

Definition 1. If M is the number of inputs to FLC and $\sigma_j \in \mathbb{R}$ is the j-th crisp variable, $j \in [1, M]$, then a type-1 FS A_j is described by a type-1 MF $\mu_A(\sigma_j) \in [0, 1]$, i.e.:

$$A_j = \{(\sigma_j, \mu(\sigma_j)) \mid \mu_A(\sigma_j) \in [0, 1] \quad \forall \sigma_j \in \mathbb{R}\}. \tag{1}$$

Three triangular type-1 FSs are illustrated in Fig. 1b.

Remark 1. If the MFs in (1) assume only 0 or 1, i.e., $\mu_A(\sigma) \in \{0, 1\}$; then, the T1-FSs degenerate into singleton FSs.

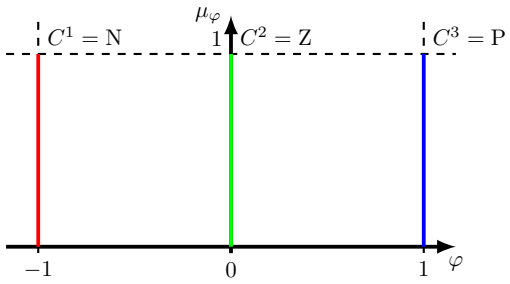

(a) (N)egative, (Z)ero and (P)ositive FSs represented by three singleton MFs.

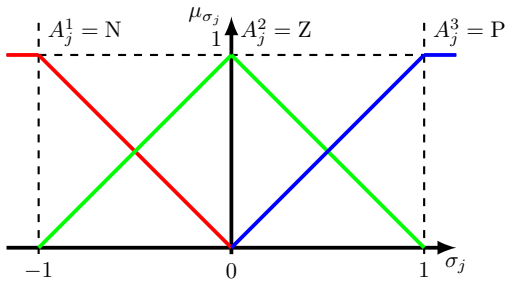

(b) (N)egative, (Z)ero and (P)ositive FSs represented by three triangular type-1 MFs.

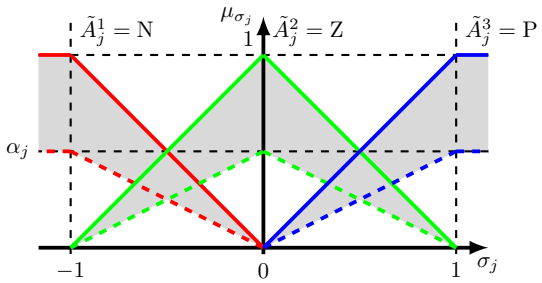

(c) (N)egative, (Z)ero and (P)ositive FSs represented by three triangular interval type-2 MFs.

Figure 1: (N)egative, (Z)ero and (P)ositive FSs represented by three (a) singleton, (b) triangular type-1, and (c) triangular interval type-2 MFs.

Three different singleton FSs are illustrated in Fig. 1a.

Definition 2. In DI-T1-FLC, a FM from $\boldsymbol{\sigma} \in \mathbb{R}^2$ to $\varphi^{\mathrm{T1}} \in \mathbb{R}$ is a function $\varphi^{\mathrm{T1}}(\boldsymbol{\sigma}) : \mathbb{R}^2 \to \mathbb{R}$, where $\boldsymbol{\sigma} = \begin{bmatrix} \sigma_1 & \sigma_2 \end{bmatrix}^T$.

Definition 3. If N is the number of rules in a rule-base R for DI-T1-FLC, then the i-th rule $R_i \in \mathrm{R}$, $i \in [1, N]$, is indicated as IF $-$ THEN statement, i.e.:

$$R_i : \text{IF } \sigma_1 \text{ is } A_{1,i} \text{ and } \sigma_2 \text{ is } A_{2,i}, \text{ THEN } \varphi^{\mathrm{T1}} \text{ is } C_i, \tag{2}$$

where C_i is a consequent FS.

A typical nine rules rule-base is shown in Table 1. In this table, the rules are sorted in ascending order w.r.t. the consequent.

Definition 4. In DI-T1-FLC, the firing strength $f_i(\boldsymbol{\sigma}) \in [0, 1]$, $i \in [1, N]$, of the i-th rule is computed with the product t-norm, i.e.:

$$f_i(\boldsymbol{\sigma}) = \mu_{A_{1,i}}(\sigma_1) \cdot \mu_{A_{2,i}}(\sigma_2). \tag{3}$$

Once the rules in (2) are defined, DI-T1-FLC can be seen as a quantitative FM from crisp inputs $\boldsymbol{\sigma}$ to crisp output φ^{T1}. In order to facilitate the analytical derivation, the antecedent MFs are designed to be triangular type-1 FSs, as illustrated in Fig. 1b. The typical representation of a triangular MF is:

$$\mu_{A_j^k}(\sigma_j) = \begin{cases} 0 & , \sigma_j < a_{k-1} \\ \frac{\sigma_j - a_{k-1}}{a_k - a_{k-1}} & , a_{k-1} \leq \sigma_j \leq a_k \\ \frac{a_{k+1} - \sigma_j}{a_{k+1} - a_k} & , a_k < \sigma_j \leq a_{k+1} \\ 0 & , \sigma_j > a_{k+1}, \end{cases} \tag{4}$$

where $k = 1, 2, 3$ and $j = 1, 2$. As can be seen from Fig. 1b, $a_0 = -\infty$, $a_1 = -1$, $a_2 = 0$, $a_3 = 1$ and $a_4 = +\infty$. In this study, to simplify the design complexity,

Table 1: A typical nine rules rule-base of DI-FLC [42].

σ_1	σ_2		
	(N)egative	(Z)ero	(P)ositive
(N)egative	R_1: (N)egative	R_2: (N)egative	R_4: (Z)ero
(Z)ero	R_3: (N)egative	R_5: (Z)ero	R_7: (P)ositive
(P)ositive	R_6: (Z)ero	R_8: (P)ositive	R_9: (P)ositive

symmetrical MFs are utilized. Besides, the consequent MFs are designed to be singleton and they are illustrated in Fig. 1a.

For our analytical analysis, complex symbolic computations are needed. Thus, an equivalent definition of (4) is used [44]:

$$\mu_{A_j^k}(\sigma_j) = \max\left(\min\left(\frac{\sigma_j - a_{k-1}}{a_k - a_{k-1}}, \frac{a_{k+1} - \sigma_j}{a_{k+1} - a_k}\right), 0\right), \tag{5}$$

where max and min functions are reformulated as algebraical functions:

$$\begin{cases} \max(a,b) &= \frac{a+b+|a-b|}{2} \\ \min(a,b) &= \frac{a+b-|a-b|}{2}. \end{cases} \tag{6}$$

The structure of double-input type-1 fuzzy proportional-derivative (DI-T1-FPD) controller, which inherits DI-T1-FLC, is shown in Fig. 2. The input scaling factors k_p and k_d are chosen to normalize e and $\dot{e}$ to the universe of discourse of the antecedent MFs, i.e., $[-1, 1]$. So, e and $\dot{e}$ are transformed into σ_1 and σ_2, respectively, before inputting them into DI-T1-FLC. Consequently, the output φ from DI-T1-FLC is transformed into the control signal v. The unscaling gain k_o is defined such that the output is denormalized to the domain of the control signal. In the adopted control structure, only one parameter has to be tuned, i.e., k_o.

2.1. Derivation of Fuzzy Mapping for DI-T1-FLC

Using the centroid defuzzification [45], the defuzzified output of T1-FLC is:

$$\varphi^{\mathrm{T1}}(\boldsymbol{\sigma}) = \frac{\sum_{i=1}^{N} f_i(\boldsymbol{\sigma}) C_i}{\sum_{i=1}^{N} f_i(\boldsymbol{\sigma})}. \tag{7}$$

Figure 2: Structure of DI-T1-FPD controller.

Table 1 contains nine rules; consequently, $N = 9$. Substituting (3) into (7):

$$\varphi^{\mathrm{T1}}(\boldsymbol{\sigma}) = \frac{\sum_{i=1}^{9} \left(\mu_{A_{1,i}}(\sigma_1) \cdot \mu_{A_{2,i}}(\sigma_2)\right) C_i}{\sum_{i=1}^{9} \mu_{A_{1,i}}(\sigma_1) \cdot \mu_{A_{2,i}}(\sigma_2)}. \tag{8}$$

Then, combining Definition 3, Table 1 and Fig. 1b, it is clear that $\mu_{A_{1,1}} = \mu_{A_{1,2}} = \mu_{A_{1,3}} = \mu_{A_{2,1}} = \mu_{A_{2,4}} = \mu_{A_{2,7}} = \mu_{A^1}$, $\mu_{A_{1,4}} = \mu_{A_{1,5}} = \mu_{A_{1,6}} = \mu_{A_{2,2}} = \mu_{A_{2,5}} = \mu_{A_{2,8}} = \mu_{A^2}$ and $\mu_{A_{1,7}} = \mu_{A_{1,8}} = \mu_{A_{1,9}} = \mu_{A_{2,3}} = \mu_{A_{2,6}} = \mu_{A_{2,9}} = \mu_{A^3}$, which are defined in (5). Combining Definition 3, Table 1 and Fig. 1a, it is clear that $C_1 = C_2 = C_4 = C^1 = -1$, $C_3 = C_5 = C_7 = C^2 = 0$ and $C_6 = C_8 = C_9 = C^3 = 1$. Hence, after performing some simplifications in (8), $\varphi^{\mathrm{T1}}(\boldsymbol{\sigma})$ is computed:

$$\varphi^{\mathrm{T1}}(\boldsymbol{\sigma}) = \sigma_1 + \sigma_2 - \frac{|\sigma_1|\sigma_2 + \sigma_1|\sigma_2|}{2}. \tag{9}$$

Remark 2. The unit mapping $\varphi^0(\boldsymbol{\sigma})$ in $[-1, 1]$ is defined as:

$$\varphi^0(\boldsymbol{\sigma}) = \frac{\sigma_1 + \sigma_2}{2}. \tag{10}$$

The expression in (9) describes DI-T1-FLC in an analytical form. Therefore, instead of considering DI-T1-FLC as a grey-box, its symbolic representation, i.e., $\varphi^{\mathrm{T1}}(\boldsymbol{\sigma})$, can be used. The generated CS, which maps the two inputs σ_1 and σ_2 to the output φ, is plotted in Fig. 3.

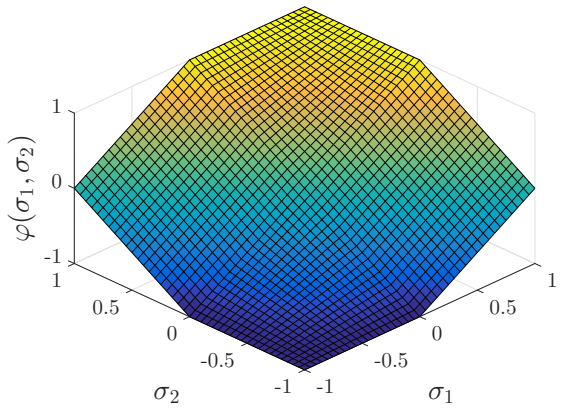

Figure 3: Control surface generated by DI-T1-FLC.

2.2. Analysis of Fuzzy Mapping for DI-T1-FLC

From the asymptotic computational analysis, the runtime complexity for T1-FLC represented by (7) is $O(2N)$ which is linear w.r.t. N. While the runtime complexity of FM for T1-FLC represented by (9) is $O(1)$ which is constant. Therefore, independently on the number of rules in the rule-base, the computational complexity of FM for T1-FLC is constant.

Definition 5. The aggressiveness ε of CS is the value of its gradient $\delta(\boldsymbol{\sigma})$ in a neighbourhood of the equilibrium point $(0,0)$ and in the direction of the unit vector $\hat{\mathbf{w}}$, i.e.:

$$\varepsilon = \hat{\mathbf{w}}^T \delta(0,0). \tag{11}$$

The gradient of $\varphi^{\mathrm{T1}}(\boldsymbol{\sigma})$ is $\delta^{\mathrm{T1}}(\boldsymbol{\sigma}) = \nabla\varphi^{\mathrm{T1}}(\boldsymbol{\sigma})$. If $\hat{\mathbf{w}} = \begin{bmatrix} \frac{1}{\sqrt{2}} & \frac{1}{\sqrt{2}} \end{bmatrix}^T$ which is the unit vector in the direction of $\begin{bmatrix} \sigma_1 & \sigma_2 \end{bmatrix}$, the aggressiveness becomes:

$$\varepsilon^{\mathrm{T1}} = \hat{\mathbf{w}}^T \delta^{\mathrm{T1}}(0,0) = \begin{bmatrix} \frac{1}{\sqrt{2}} & \frac{1}{\sqrt{2}} \end{bmatrix} \begin{bmatrix} 1 \\ 1 \end{bmatrix} = \sqrt{2}. \tag{12}$$

Remark 3. If the gradient of $\varphi^0(\boldsymbol{\sigma})$ is $\delta^0(\boldsymbol{\sigma}) = \nabla\varphi^0(\boldsymbol{\sigma})$, then the aggressiveness of the unit mapping in (10) is

$$\varepsilon^0 = \hat{\mathbf{w}}^T \delta^0(0,0) = \begin{bmatrix} \frac{1}{\sqrt{2}} & \frac{1}{\sqrt{2}} \end{bmatrix} \begin{bmatrix} 1/2 \\ 1/2 \end{bmatrix} = \frac{\sqrt{2}}{2}. \tag{13}$$

From (12) and (13), it can be observed that $\varphi^{\mathrm{T1}}(\boldsymbol{\sigma})$ is more aggressive than $\varphi^0(\boldsymbol{\sigma})$ in the neighbourhood of $(0,0)$, since $\varepsilon^{\mathrm{T1}} > \varepsilon^0$.

Theorem 1. *If $\varphi^{\mathrm{T1}}(\boldsymbol{\sigma})$ indicates FM of DI-T1-FLC, then*

i) $\varphi^{\mathrm{T1}}(\sigma_1, \sigma_2)$ is an even symmetric function w.r.t. the bisection of the first ($\sigma_1 > 0$, $\sigma_2 > 0$) and third ($\sigma_1 < 0$, $\sigma_2 < 0$) quadrants in the Cartesian plane, i.e., $\varphi^{\mathrm{T1}}(\sigma_1, \sigma_2) = \varphi^{\mathrm{T1}}(\sigma_2, \sigma_1) \quad \forall\sigma_1 \in [-1,1] \quad \forall\sigma_2 \in [-1,1]$;

ii) $\varphi^{\mathrm{T1}}(\sigma_1, \sigma_2)$ is an odd symmetric function w.r.t. the bisection of the second ($\sigma_1 > 0$, $\sigma_2 < 0$) and fourth ($\sigma_1 < 0$, $\sigma_2 > 0$) quadrants in the Cartesian plane, i.e., $\varphi^{\mathrm{T1}}(-\sigma_1, -\sigma_2) = -\varphi^{\mathrm{T1}}(\sigma_1, \sigma_2) \quad \forall\sigma_1 \in [-1,1] \quad \forall\sigma_2 \in [-1,1]$.

Proof. Using (9), it follows:

i) $\varphi^{\mathrm{T1}}(\sigma_1,\sigma_2)=\sigma_1+\sigma_2-\frac{|\sigma_1|\sigma_2+\sigma_1|\sigma_2|}{2}$ and $\varphi^{\mathrm{T1}}(\sigma_2,\sigma_1)=\sigma_2+\sigma_1-\frac{|\sigma_2|\sigma_1+\sigma_2|\sigma_1|}{2}$; therefore, $\varphi^{\mathrm{T1}}(\sigma_1,\sigma_2)=\varphi^{\mathrm{T1}}(\sigma_2,\sigma_1) \quad \forall\sigma_1\in[-1,1] \quad \forall\sigma_2\in[-1,1]$;

ii) $\varphi^{\mathrm{T1}}(-\sigma_1,-\sigma_2)=-\sigma_1-\sigma_2-\frac{-|\sigma_1|\sigma_2-\sigma_1|\sigma_2|}{2}=-\sigma_1-\sigma_2+\frac{|\sigma_1|\sigma_2+\sigma_1|\sigma_2|}{2}=-\varphi^{\mathrm{T1}}(\sigma_1,\sigma_2)$; therefore, $\varphi^{\mathrm{T1}}(-\sigma_1,-\sigma_2) = -\varphi^{\mathrm{T1}}(\sigma_1,\sigma_2) \quad \forall\sigma_1 \in [-1,1] \quad \forall\sigma_2\in[-1,1]$.

□

Corollary 1. *Using the second property in Theorem 1, $\varphi^{\mathrm{T1}}(\boldsymbol{\sigma})$ can be rewritten as:*

$$\varphi^{\mathrm{T1}}(\boldsymbol{\sigma})=-\varphi^{\mathrm{T1}}(-\boldsymbol{\sigma}). \tag{14}$$

Theorem 2. *If $\varphi^{\mathrm{T1}}(\boldsymbol{\sigma})$ indicates FM of DI-T1-FLC, then $\varphi^{\mathrm{T1}}(\boldsymbol{\sigma})$ is a continuous function in the region $[-1,1]^2$ w.r.t. its input variable $\boldsymbol{\sigma}$, i.e., $\varphi^{\mathrm{T1}} \in \mathcal{C}^0([-1,1]^2)$.*

Proof. First, (9) is decomposed into two components: $\varphi^{\mathrm{T1},1}(\boldsymbol{\sigma})=\sigma_1+\sigma_2$ and $\varphi^{\mathrm{T1},2}(\boldsymbol{\sigma})=\frac{|\sigma_1|\sigma_2+\sigma_1|\sigma_2|}{2}$. Since $\varphi^{\mathrm{T1},1}(\boldsymbol{\sigma})$ is a polynomial function, it is continuous on $\mathbb{R}^2$. On the other side, it can be observed that $\lim_{\sigma_1\to\mathbf{c}}\varphi^{\mathrm{T1},2}(\boldsymbol{\sigma})=\varphi^{\mathrm{T1},2}(\mathbf{c}) \quad \forall\mathbf{c}\in\mathbb{R}^2$. Therefore, $\varphi^{\mathrm{T1},2}(\boldsymbol{\sigma})$ is also continuous on $\mathbb{R}^2$. Since $\varphi^{\mathrm{T1}}(\boldsymbol{\sigma})$ is a linear combination of continuous functions, i.e., $\varphi^{\mathrm{T1}}(\boldsymbol{\sigma})=\varphi^{\mathrm{T1},1}(\boldsymbol{\sigma})-\varphi^{\mathrm{T1},2}(\boldsymbol{\sigma})$, $\varphi^{\mathrm{T1}}(\boldsymbol{\sigma})$ is also a continuous function.

□

Theorem 3. *If $\varphi^{\mathrm{T1}}(\boldsymbol{\sigma})$ indicates FM of DI-T1-FLC, then $\varphi^{\mathrm{T1}}(\boldsymbol{\sigma})$ is a monotonic increasing function in the region $[-1,1]^2$ w.r.t. its input variables $\boldsymbol{\sigma}$, i.e., $\frac{\partial\varphi^{\mathrm{T1}}}{\partial\sigma_1}\geq 0 \wedge \frac{\partial\varphi^{\mathrm{T1}}}{\partial\sigma_2}\geq 0 \quad \forall\boldsymbol{\sigma}\in[-1,1]^2$.*

Proof. Initially, let's prove that $\varphi(\boldsymbol{\sigma})$ is an increasing function w.r.t. σ_1 $\forall\boldsymbol{\sigma}\in[-1,1]^2$. From 9, $\frac{\partial\varphi^{\mathrm{T1}}}{\partial\sigma_1}=1-\frac{\sigma_2\mathrm{sign}(\sigma_1)-|\sigma_2|}{2}$. By observing that $|\sigma_2|=\sigma_2\mathrm{sign}(\sigma_2)$, $\frac{\partial\varphi^{\mathrm{T1}}}{\partial\sigma_1}=1-\frac{\sigma_2(\mathrm{sign}(\sigma_1)-\mathrm{sign}(\sigma_2))}{2}$, in which $\frac{\sigma_2(\mathrm{sign}(\sigma_1)-\mathrm{sign}(\sigma_2))}{2}\in[-1,1] \quad \forall\boldsymbol{\sigma}\in[-1,1]^2$. Consequently, $\frac{\partial\varphi^{\mathrm{T1}}}{\partial\sigma_1}\in[0,2] \quad \forall\boldsymbol{\sigma}\in[-1,1]^2$, and, thus, $\frac{\partial\varphi^{\mathrm{T1}}}{\partial\sigma_1}\geq 0 \quad \forall\boldsymbol{\sigma}\in$

$[-1,1]^2$. From the first result in Theorem 1, if $\frac{\partial \varphi^{\mathrm{T1}}}{\partial \sigma_1} \geq 0 \quad \forall \boldsymbol{\sigma} \in [-1,1]^2$, then $\frac{\partial \varphi^{\mathrm{T1}}}{\partial \sigma_2} \geq 0 \quad \forall \boldsymbol{\sigma} \in [-1,1]^2$. Therefore, φ^{T1} is a monotonic increasing in the region $[-1,1]^2$ w.r.t. its input variables σ_1 and σ_2.

□

3. Double-Input Interval Type-2 Fuzzy Logic Controller

First of all, some important definitions for IT2-FLC are reviewed, which will allow to introduce DI-IT2-FLC.

Definition 6. In type-2 FS $\tilde{A}$, the upper MF $\overline{\mu}_{\tilde{A}}(\sigma_j) \forall \sigma_j \in \mathbb{R}$ is MF which confines from top FOU($\tilde{A}$) (coloured solid lines in Fig. 1c); while the lower MF $\underline{\mu}_{\tilde{A}}(\sigma_j) \forall \sigma_j \in \mathbb{R}$ is MF which confines from bottom FOU($\tilde{A}$) (coloured dashed lines in Fig. 1c), i.e.:

$$\begin{cases} \overline{\mu}_{\tilde{A}}(\sigma_j) = \sup\{u \mid \mu_{\tilde{A}}(\sigma_j, u) > 1\} \quad \forall \sigma_j \in \mathbb{R} \quad \forall u \in [0,1] \\ \underline{\mu}_{\tilde{A}}(\sigma_j) = \inf\{u \mid \mu_{\tilde{A}}(\sigma_j, u) > 1\} \quad \forall \sigma_j \in \mathbb{R} \quad \forall u \in [0,1]. \end{cases} \tag{15}$$

Definition 7. If $U \equiv \left[\overline{\mu}_{\tilde{A}}(\sigma_j), \underline{\mu}_{\tilde{A}}(\sigma_j)\right] \forall \sigma_j \in \mathbb{R}$ is the universe of the secondary variable $u \in U$, then an interval type-2 FS $\tilde{A}$ is described by an interval type-2 MF, i.e.:

$$\tilde{A} = \{(\sigma_j, u, 1) \quad \forall \sigma_j \in \mathbb{R} \quad \forall u \in U\}. \tag{16}$$

Definition 8. In interval type-2 FS $\tilde{A}$, FOU is a limited region (grey areas in Fig. 1c) which is defined by the union of all $\mu_{\tilde{A}}(\sigma_j, u) = 1$, i.e.:

$$\mathrm{FOU}(\tilde{A}) = \left\{(\sigma_j, u) \quad \forall \sigma_j \in \mathbb{R} \quad \forall u \in U \equiv \left[\underline{\mu}_{\tilde{A}}(\sigma_j), \overline{\mu}_{\tilde{A}}(\sigma_j)\right]\right\}. \tag{17}$$

Definition 9. In DI-IT2-FLC, FM from $\boldsymbol{\sigma} \in \mathbb{R}^2$ to $\varphi^{\mathrm{IT2}} \in \mathbb{R}$ is a function $\varphi^{\mathrm{IT2}}(\boldsymbol{\sigma}) : \mathbb{R}^2 \to \mathbb{R}$, where $\boldsymbol{\sigma} = \begin{bmatrix} \sigma_1 & \sigma_2 \end{bmatrix}^T$.

Definition 10. In DI-IT2-FLC, the i-th rule $R_i \in \mathrm{R}$, $i \in [1, N]$, is indicated as IF − THEN statement, i.e.:

$$R_i : \text{IF } \sigma_1 \text{ is } \tilde{A}_{1,i} \text{ and } \sigma_2 \text{ is } \tilde{A}_{2,i}, \text{ THEN } \varphi^{\mathrm{IT2}} \text{ is } C_i. \tag{18}$$

Definition 11. In DI-IT2-FLC, the set of firing strengths $F_i(\boldsymbol{\sigma}) \in [0,1]^2$, $i \in [1, N]$, of the i-th rule is computed with the product t-norm:

$$F_i(\boldsymbol{\sigma}) = \begin{bmatrix} \overline{f}_i(\boldsymbol{\sigma}) = \overline{\mu}_{A_{1,i}}(\sigma_1) \cdot \overline{\mu}_{A_{2,i}}(\sigma_2) \\ \underline{f}_i(\boldsymbol{\sigma}) = \underline{\mu}_{A_{1,i}}(\sigma_1) \cdot \underline{\mu}_{A_{2,i}}(\sigma_2) \end{bmatrix}. \tag{19}$$

Once the rules in (18) are defined, DI-IT2-FLC becomes a quantitative FM from crisp inputs $\boldsymbol{\sigma}$ to crisp output φ^{IT2}. To facilitate the analytical derivation, the antecedent MFs are designed to be triangular interval type-2 FSs, as depicted in Fig. 1c. As illustrated in Fig. 1c, DI-IT2-FLC employs completely overlapping interval type-2 FSs. Consequently, it is ensured that each input σ_j always belong to one or two FSs.

In this study, to simplify the design complexity, symmetrical MFs are utilized. The common way to represent triangular interval type-2 FSs is:

$$\begin{cases} \overline{\mu}_{\tilde{A}_j^k}(\sigma_j) & = \mu_{A_j^k}(\sigma_j) \\ \underline{\mu}_{\tilde{A}_j^k}(\sigma_j) & = \alpha_j \mu_{A_j^k}(\sigma_j), \end{cases} \tag{20}$$

where α_j is the height of the lower MFs and the only parameter to tune [33]. Such a simplification will bring significant advantages when designing a controller.

Remark 4. If $\alpha_j = 1 \quad \forall j$, then $\overline{\mu}_{\tilde{A}_{j,k}}(\sigma_j) \equiv \underline{\mu}_{\tilde{A}_{j,k}}(\sigma_j)$ and interval type-2 FSs will degenerate to type-1 FSs.

The structure of double-input interval type-2 fuzzy proportional-derivative (DI-IT2-FPD) controller, which inherits DI-IT2-FLC with α_1 and α_2, is depicted in Fig. 4. The input scaling factors k_p and k_d are chosen to normalize e and $\dot{e}$

Figure 4: Structure of DI-IT2-FPD controller.

to the universe of discourse of the antecedent MFs, i.e., $[-1, 1]$. The unscaling gain k_o is defined such that the output is denormalized to the domain of the control signal. In the adopted control structure, three parameters have to be tuned, i.e., α_1, α_2 and k_o.

3.1. Derivation of Fuzzy Mapping for DI-IT2-FLC

By using the defuzzification and type-reduction, the defuzzified output of IT2-FLC is, as in [46]:

$$\varphi^{\mathrm{IT2}}(\boldsymbol{\sigma}) = \frac{\varphi_L(\boldsymbol{\sigma}) + \varphi_R(\boldsymbol{\sigma})}{2}, \tag{21}$$

in which φ_L and φ_R are left and right endpoints of the type-reduced set, respectively. Consequently, it is possible to calculate φ_L and φ_R with KM centroid type-reduction algorithm [47]:

$$\begin{cases} \varphi_L(\boldsymbol{\sigma}) & = \frac{\sum_{i=1}^{L} \overline{f}_i(\boldsymbol{\sigma}) C_i + \sum_{i=L+1}^{N} \underline{f}_i(\boldsymbol{\sigma}) C_i}{\sum_{i=1}^{L} \overline{f}_i(\boldsymbol{\sigma}) + \sum_{i=L+1}^{N} \underline{f}_i(\boldsymbol{\sigma})} \\ \varphi_R(\boldsymbol{\sigma}) & = \frac{\sum_{i=1}^{R} \underline{f}_i(\boldsymbol{\sigma}) C_i + \sum_{i=R+1}^{N} \overline{f}_i(\boldsymbol{\sigma}) C_i}{\sum_{i=1}^{R} \underline{f}_i(\boldsymbol{\sigma}) + \sum_{i=R+1}^{N} \overline{f}_i(\boldsymbol{\sigma})}, \end{cases} \tag{22}$$

in which L and R are the left and right switching points, respectively. Usually, L and R are computed by an iterative algorithm. Nevertheless, by observing the structure of the rule-base for double-input FLC in Table 1, each consequent MF (N, Z, P) can be implied from exactly three rules. Consequently, L and R are multiples of 3 in interval $(1, 9)$, i.e., $L \in \{3, 6\} \wedge R \in \{3, 6\}$. By using the constraint that $L \leq R$, three distinct cases for the switching points can be determined, i.e., $< \{L = 3, R = 3\}, \{L = 3, R = 6\}, \{L = 6, R = 6\} >$. Each of these cases defines a region (Ω_1, Ω_2, Ω_3) on $[\sigma_1 \times \sigma_2]$ plane, as shown in Fig. 5. Hence, Ω_1, Ω_2 and Ω_3 are analytically defined as:

$$\begin{cases} \Omega_1 = \left\{ \{\sigma_1, \sigma_2\} \in [-1, 1]^2 \mid \sigma_2 \geq -1, \sigma_2 \leq \omega_{12}(\sigma_1) \right\} \\ \Omega_2 = \left\{ \{\sigma_1, \sigma_2\} \in [-1, 1]^2 \mid \sigma_2 > \omega_{12}(\sigma_1), \sigma_2 < \omega_{23}(\sigma_1) \right\} \\ \Omega_3 = \left\{ \{\sigma_1, \sigma_2\} \in [-1, 1]^2 \mid \sigma_2 \geq \omega_{23}(\sigma_1), \sigma_2 \leq 1 \right\}, \end{cases} \tag{23}$$

where ω_{12} and ω_{23} are the contours which separate Ω_1 from Ω_2 and Ω_2 from Ω_3, respectively. For each region corresponds FM, i.e., $\varphi_1^{\mathrm{IT2}}(\boldsymbol{\sigma})$, $\varphi_2^{\mathrm{IT2}}(\boldsymbol{\sigma})$ and

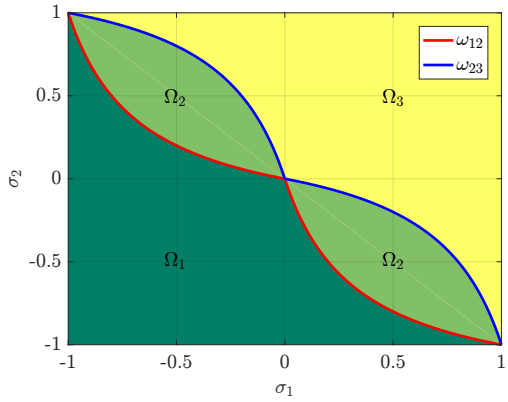

Figure 5: Three regions of DI-IT2-FLC FM and two contours between them.

$\varphi_3^{\mathrm{IT2}}(\boldsymbol{\sigma})$. Thus, $\varphi^{\mathrm{IT2}}(\boldsymbol{\sigma})$ can be broken down by using (21):

$$\varphi^{\mathrm{IT2}}(\boldsymbol{\sigma}) = \begin{cases} \varphi_1^{\mathrm{IT2}}(\boldsymbol{\sigma}) = \frac{\varphi_{L=3}(\boldsymbol{\sigma})+\varphi_{R=3}(\boldsymbol{\sigma})}{2}, \boldsymbol{\sigma} \in \Omega_1 \\ \varphi_2^{\mathrm{IT2}}(\boldsymbol{\sigma}) = \frac{\varphi_{L=3}(\boldsymbol{\sigma})+\varphi_{R=6}(\boldsymbol{\sigma})}{2}, \boldsymbol{\sigma} \in \Omega_2 \\ \varphi_3^{\mathrm{IT2}}(\boldsymbol{\sigma}) = \frac{\varphi_{L=6}(\boldsymbol{\sigma})+\varphi_{R=6}(\boldsymbol{\sigma})}{2}, \boldsymbol{\sigma} \in \Omega_3. \end{cases} \tag{24}$$

The determination of the he left and right end points allows to derive the output of DI-IT2-FLC in a closed-form. Therefore, it is possible to find the FM $\varphi(\boldsymbol{\sigma})$ by substituting (19) into (22):

$$\begin{cases} \varphi_{L=3}(\boldsymbol{\sigma}) &= \frac{\sigma_1(\sigma_2+1)-\sigma_1\sigma_2+\sigma_2(\sigma_1+1)}{\alpha_1\alpha_2(\sigma_1+1)(\sigma_2+1)-\sigma_1-\sigma_2(\sigma_1+1)} \\ \varphi_{L=6}(\boldsymbol{\sigma}) &= \frac{\alpha_1\alpha_2\sigma_2-\alpha_1\alpha_2\sigma_1(\sigma_2-1)}{(\sigma_1-1)(\sigma_2-1)+\alpha_1\alpha_2(\sigma_1+\sigma_2-\sigma_2\sigma_1)} \\ \varphi_{R=3}(\boldsymbol{\sigma}) &= \frac{\alpha_1\alpha_2\sigma_1+\alpha_1\alpha_2\sigma_2(\sigma_1+1)}{(\sigma_1+1)(\sigma_2+1)-\alpha_1\alpha_2(\sigma_1\sigma_2+\sigma_1+\sigma_2)} \\ \varphi_{R=6}(\boldsymbol{\sigma}) &= \frac{\sigma_1(1-\sigma_2)+\sigma_1\sigma_2-\sigma_2(1-\sigma_1)}{\alpha_1\alpha_2(\sigma_1-1)(\sigma_2-1)-\sigma_1-\sigma_2(\sigma_1-1)}, \end{cases} \tag{25}$$

Now, $\varphi_1^{\mathrm{IT2}}(\boldsymbol{\sigma})$, $\varphi_2^{\mathrm{IT2}}(\boldsymbol{\sigma})$ and $\varphi_3^{\mathrm{IT2}}(\boldsymbol{\sigma})$ are computed with (24):

$$\begin{cases} \varphi_1^{\mathrm{IT2}}(\boldsymbol{\sigma}) & = \frac{1}{2}\frac{\alpha_1\alpha_2(\sigma_1\sigma_2-\sigma_1-\sigma_2)}{(\sigma_1-1)(\sigma_2-1)+\alpha_1\alpha_2(\sigma_1+\sigma_2-\sigma_2\sigma_1)} \\ & \quad +\frac{1}{2}\frac{\sigma_1\sigma_2-\sigma_1-\sigma_2}{\alpha_1\alpha_2(\sigma_1-1)(\sigma_2-1)+\sigma_1+\sigma_2-\sigma_1\sigma_2} \\ \varphi_2^{\mathrm{IT2}}(\boldsymbol{\sigma}) & = \frac{1}{2}\frac{\sigma_2(\sigma_1+1)-\alpha_1\alpha_2\sigma_1(\sigma_2-1)}{\sigma_2(\sigma_1+1)-\alpha_1\alpha_2\sigma_1-\alpha_1\alpha_2(\sigma_1+1)(\sigma_2-1)} \\ & \quad -\frac{1}{2}\frac{\sigma_1(\sigma_2-1)-\alpha_1\alpha_2\sigma_2(\sigma_1+1)}{\sigma_1(\sigma_2-1)+\alpha_1\alpha_2\sigma_2-\alpha_1\alpha_2(\sigma_1+1)(\sigma_2-1)} \\ \varphi_3^{\mathrm{IT2}}(\boldsymbol{\sigma}) & = \frac{1}{2}\frac{\alpha_1\alpha_2(\sigma_1+\sigma_2-\sigma_1\sigma_2)}{(\sigma_1-1)(\sigma_2-1)+\alpha_1\alpha_2\sigma_1-\alpha_1\alpha_2\sigma_2(\sigma_1-1)} \\ & \quad -\frac{1}{2}\frac{\sigma_1\sigma_2-\sigma_1-\sigma_2}{\sigma_1+\sigma_2-\sigma_1\sigma_2+\alpha_1\alpha_2(\sigma_1-1)(\sigma_2-1)}. \end{cases} \tag{26}$$

Finally, by definition the contours which separate Ω_1 from Ω_2 and Ω_2 from Ω_3, respectively, are:

$$\begin{cases} \omega_{12} & = \left\{\boldsymbol{\sigma} \in [-1,1]^2 \mid \varphi_{R=3}(\boldsymbol{\sigma}) = \varphi_{R=6}(\boldsymbol{\sigma})\right\} \\ \omega_{23} & = \left\{\boldsymbol{\sigma} \in [-1,1]^2 \mid \varphi_{L=3}(\boldsymbol{\sigma}) = \varphi_{L=6}(\boldsymbol{\sigma})\right\}, \end{cases} \tag{27}$$

ω_{12} and ω_{23} are computed as functions of only σ_1 with (25):

$$\omega_{12}(\sigma_1) = \begin{cases} \frac{-\alpha_1\alpha_2\sigma_1}{\sigma_1-\alpha_1\alpha_2\sigma_1+1}, & \sigma_1 < 0 \\ \frac{-\sigma_1}{\sigma_1+\alpha_1\alpha_2-\alpha_1\alpha_2\sigma_1}, & \sigma_1 \geq 0 \end{cases} \tag{28}$$

and

$$\omega_{23}(\sigma_1) = \begin{cases} \frac{-\sigma_1}{\alpha_1\alpha_2-\sigma_1+\alpha_1\alpha_2\sigma_1}, & \sigma_1 < 0 \\ \frac{-\alpha_1\alpha_2\sigma_1}{\alpha_1\alpha_2\sigma_1-\sigma_1+1}, & \sigma_1 \geq 0. \end{cases} \tag{29}$$

Therefore, instead of considering DI-IT2-FLC as a gray-box, its explicit representation in (24), i.e., $\varphi^{\mathrm{IT2}}(\boldsymbol{\sigma})$, can be used.

Remark 5. If $\alpha_1 = 1$ and $\alpha_2 = 1$, then $\varphi^{\mathrm{IT2}}(\boldsymbol{\sigma})$ in (26) will become $\varphi^{\mathrm{T1}}(\boldsymbol{\sigma})$ in (9).

Remark 6. It can be observed from (25), (26), (28) and (29) that α_1 and α_2 are always coupled, i.e., $\alpha_1\alpha_2$. Therefore, it makes sense to perform the analysis only w.r.t. $\alpha = \alpha_1\alpha_2$. The reason why α_1 and α_2 are always coupled is because the meet operation used to compute the lower firing strengths $\underline{f}_i(\boldsymbol{\sigma})$, $i \in [1, N]$, in (19), is the product t-norm.

3.2. Analysis of Fuzzy Mapping for DI-IT2-FLC

From the asymptotic computational analysis, the runtime complexity for IT2-FLC represented by (21) and (22) is $O(4N)$ which is still linear w.r.t. N. While the runtime complexity of FM for IT2-FLC represented by (26) is $O(1)$ which is constant. Therefore, independently on the number of rules in the rule-base, the computational complexity of FM for IT2-FLC is constant in N.

The gradient of $\varphi^{\mathrm{IT2}}(\boldsymbol{\sigma})$ is $\delta^{\mathrm{IT2}}(\boldsymbol{\sigma}) = \nabla\varphi^{\mathrm{IT2}}(\boldsymbol{\sigma})$. By using Definition 5, the aggressiveness of $\varphi^{\mathrm{IT2}}(\boldsymbol{\sigma})$ can by computed as:

$$\varepsilon^{\mathrm{IT2}} = \hat{\mathbf{w}}^T \delta^{\mathrm{IT2}}(0,0) = \frac{\sqrt{2}}{2}\left(\alpha + \frac{1}{\alpha}\right). \tag{30}$$

This relation is depicted in Fig. 6. For small values of α, the behaviour of DI-IT2-FLC becomes more aggressive around $(0,0)$; while, for high values of α, the behaviour of DI-IT2-FLC becomes less aggressive around $(0,0)$.

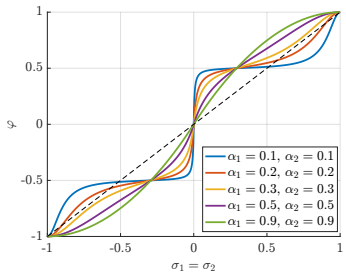

Figure 6: Relation between aggressiveness of $\varphi^{\mathrm{IT2}}(\boldsymbol{\sigma})$ and α.

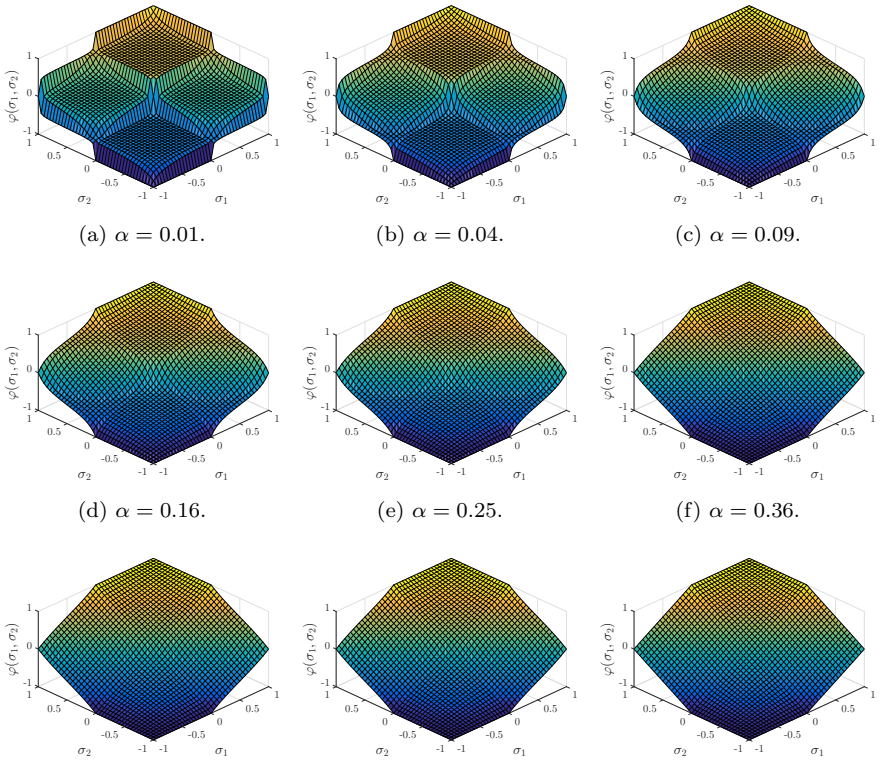

(a) $\alpha = 0.01$. (b) $\alpha = 0.04$. (c) $\alpha = 0.09$.

(d) $\alpha = 0.16$. (e) $\alpha = 0.25$. (f) $\alpha = 0.36$.

(g) $\alpha = 0.49$. (h) $\alpha = 0.64$. (i) $\alpha = 0.81$.

Figure 7: Control surface generated by DI-IT2-FLC for different values of α. The values for α are chosen using the relations $\alpha = \alpha_1\alpha_2$ and $\alpha_1 = \alpha_2$, where $\alpha_1 \in \{0.1, 0.2, 0.3, 0.4, 0.5, 0.6, 0.7, 0.8, 0.9\}$.

Remark 7. It is noted that $\varphi^{\mathrm{T1}}(\boldsymbol{\sigma})$ is not more aggressive than $\varphi^{\mathrm{IT2}}(\boldsymbol{\sigma})$, since $\varepsilon^{\mathrm{IT2}} \geq \varepsilon^{\mathrm{T1}} \quad \forall\alpha$ and $\varepsilon^{\mathrm{IT2}} = \varepsilon^{\mathrm{T1}}$ only when $\alpha = 1$. Consequently, it is noted that $\varphi^{0}(\boldsymbol{\sigma})$ is less aggressive than $\varphi^{\mathrm{IT2}}(\boldsymbol{\sigma})$, since $\varepsilon^{\mathrm{IT2}} > \varepsilon^{0} \quad \forall\alpha$.

The generated CSs, which map σ_1 and σ_2 to $\varphi^{\mathrm{IT2}}(\sigma_1, \sigma_2)$, are plotted in Fig. 7 for $\alpha_1 \in \{0.1, 0.2, 0.3, 0.4, 0.5, 0.6, 0.7, 0.8, 0.9\}$. Distinct CSs can be generated by simply varying only one parameter of FOU, i.e., α.

Theorem 4. *If $\varphi^{\mathrm{IT2}}(\boldsymbol{\sigma})$ indicates FM of DI-IT2-FLC, then*

i) $\varphi^{\mathrm{IT2}}(\sigma_1, \sigma_2)$ is an even symmetric function w.r.t. the bisection of the first ($\sigma_1 > 0$, $\sigma_2 > 0$) and third ($\sigma_1 < 0$, $\sigma_2 < 0$) quadrants in the Cartesian

plane, i.e., $\varphi^{\mathrm{IT2}}(\sigma_1,\sigma_2)=\varphi^{\mathrm{IT2}}(\sigma_2,\sigma_1)\quad\forall\sigma_1\in[-1,1]\quad\forall\sigma_2\in[-1,1]$*;*

ii) $\varphi^{\mathrm{IT2}}(\sigma_1,\sigma_2)$ *is an odd symmetric function w.r.t. the bisection of the second* ($\sigma_1>0$, $\sigma_2<0$) *and fourth* ($\sigma_1<0$, $\sigma_2>0$) *quadrants in the Cartesian plane, i.e.,* $\varphi^{\mathrm{IT2}}(-\sigma_1,-\sigma_2)=-\varphi^{\mathrm{IT2}}(\sigma_1,\sigma_2)\quad\forall\sigma_1\in[-1,1]\quad\forall\sigma_2\in[-1,1]$.

Proof.

i) To prove this property, the sufficient and necessary conditions are $\varphi_1^{\mathrm{IT2}}(\sigma_1,\sigma_2)=\varphi_1^{\mathrm{IT2}}(\sigma_2,\sigma_1)$, $\varphi_2^{\mathrm{IT2}}(\sigma_1,\sigma_2)=\varphi_2^{\mathrm{IT2}}(\sigma_2,\sigma_1)$ and $\varphi_3^{\mathrm{IT2}}(\sigma_1,\sigma_2)=\varphi_3^{\mathrm{IT2}}(\sigma_2,\sigma_1)$, which is immediate from (26).

ii) To prove this property, the sufficient and necessary conditions are $\varphi_1^{\mathrm{IT2}}(-\sigma_1,-\sigma_2)=-\varphi_1^{\mathrm{IT2}}(\sigma_1,\sigma_2)$ and $\varphi_2^{\mathrm{IT2}}(-\sigma_1,-\sigma_2)=-\varphi_2^{\mathrm{IT2}}(\sigma_1,\sigma_2)$, which is immediate from (26).

□

Corollary 2. *Using the second property in Theorem 4,* $\varphi_3(\boldsymbol{\sigma})$ *can be rewritten as:*

$$\varphi_3(\boldsymbol{\sigma})=-\varphi_1(-\boldsymbol{\sigma}). \tag{31}$$

Lemma 1. *If* $\varphi_{L=3}(\boldsymbol{\sigma})$, $\varphi_{L=6}(\boldsymbol{\sigma})$, $\varphi_{R=3}(\boldsymbol{\sigma})$ *and* $\varphi_{R=6}(\boldsymbol{\sigma})$ *indicate left and right FMs of the type-reduced set,* ω_{12} *and* ω_{23} *are the switching borders between* $\varphi_{R=3}(\boldsymbol{\sigma})$ *and* $\varphi_{R=6}(\boldsymbol{\sigma})$ *and between* $\varphi_{L=3}(\boldsymbol{\sigma})$ *and* $\varphi_{L=6}(\boldsymbol{\sigma})$*, respectively, then*

$$\begin{cases}\varphi_{L=3}(\boldsymbol{\sigma})=\varphi_{L=6}(\boldsymbol{\sigma})=0\mid\sigma_2=\omega_{23}(\sigma_1)\quad\forall\sigma_1\\ \varphi_{R=3}(\boldsymbol{\sigma})=\varphi_{R=6}(\boldsymbol{\sigma})=0\mid\sigma_2=\omega_{12}(\sigma_1)\quad\forall\sigma_1.\end{cases} \tag{32}$$

Proof. By substituting (28) and (29) into (25), it is possible to observe that $\varphi_{R=3}(\sigma_1,\omega_{12}(\sigma_1))=0\wedge\varphi_{R=6}(\sigma_1,\omega_{12}(\sigma_1))=0\wedge\varphi_{L=3}(\sigma_1,\omega_{23}(\sigma_1))=0\wedge\varphi_{L=6}(\sigma_1,\omega_{23}(\sigma_1))=0$.

□

Theorem 5. *If* $\varphi^{\mathrm{IT2}}(\boldsymbol{\sigma})$ *indicates FM of DI-IT2-FLC, then* $\varphi^{\mathrm{IT2}}(\boldsymbol{\sigma})$ *is a continuous function in the region* $[-1,1]^2$ *w.r.t. its input variable* $\boldsymbol{\sigma}$*, i.e.,* $\varphi^{\mathrm{IT2}}\in\mathcal{C}^0([-1,1]^2)$.

Proof. As can be observed from (25), no vertical asymptotes exist in $\varphi_{L=3}(\boldsymbol{\sigma})$, $\varphi_{L=6}(\boldsymbol{\sigma})$, $\varphi_{R=3}(\boldsymbol{\sigma})$ and $\varphi_{R=6}(\boldsymbol{\sigma})$ in their domains of definition $\Omega_1 \cup \Omega_2$, Ω_3, Ω_1 and $\Omega_2 \cup \Omega_3$, respectively. Namely, $\lim_{\boldsymbol{\sigma}\to\mathbf{c}} \varphi_{L=3}(\boldsymbol{\sigma}) = \varphi_{L=3}(\mathbf{c}) \quad \forall \boldsymbol{\sigma} \in \Omega_1 \cup \Omega_2 \wedge \lim_{\boldsymbol{\sigma}\to\mathbf{c}} \varphi_{L=6}(\boldsymbol{\sigma}) = \varphi_{L=6}(\mathbf{c}) \quad \forall \boldsymbol{\sigma} \in \Omega_3 \wedge \lim_{\boldsymbol{\sigma}\to\mathbf{c}} \varphi_{R=3}(\boldsymbol{\sigma}) = \varphi_{R=3}(\mathbf{c}) \quad \forall \boldsymbol{\sigma} \in \Omega_1 \wedge \lim_{\boldsymbol{\sigma}\to\mathbf{c}} \varphi_{R=6}(\boldsymbol{\sigma}) = \varphi_{R=6}(\mathbf{c}) \quad \forall \boldsymbol{\sigma} \in \Omega_2 \cup \Omega_3$. Therefore, $\varphi_{L=3}(\boldsymbol{\sigma})$ is continuous on $\Omega_1 \cup \Omega_2$, $\varphi_{L=6}(\boldsymbol{\sigma})$ is continuous on Ω_3, $\varphi_{R=3}(\boldsymbol{\sigma})$ is continuous on Ω_1 and $\varphi_{L=6}(\boldsymbol{\sigma})$ is continuous on $\Omega_2 \cup \Omega_3$.

Besides, by using Lemma 1, $\lim_{\boldsymbol{\sigma}\to\mathbf{c}} \varphi_{L=3}(\boldsymbol{\sigma}) = \lim_{\boldsymbol{\sigma}\to\mathbf{c}} \varphi_{L=6}(\boldsymbol{\sigma}) = 0 \quad \forall \mathbf{c} = [c_1, c_2] \mid c_2 = \omega_{23}(c_1) \wedge \lim_{\boldsymbol{\sigma}\to\mathbf{c}} \varphi_{R=3}(\boldsymbol{\sigma}) = \lim_{\boldsymbol{\sigma}\to\mathbf{c}} \varphi_{R=6}(\boldsymbol{\sigma}) = 0 \quad \forall \mathbf{c} = [c_1, c_2] \mid c_2 = \omega_{12}(c_1)$. Thus, also the continuity on the border ω_{23} for $\varphi_L(\boldsymbol{\sigma})$ and on the border ω_{12} for $\varphi_R(\boldsymbol{\sigma})$ is proven. Therefore, $\varphi_L(\boldsymbol{\sigma})$ and $\varphi_R(\boldsymbol{\sigma})$ are continuous in the region $[-1,1]^2$, i.e., $\varphi_L \in \mathcal{C}^0([-1,1]^2) \wedge \varphi_R \in \mathcal{C}^0([-1,1]^2)$.

Lastly, the Theorem of Continuous Functions states that "the sum of a finite number of continuous functions is a continuous function". From (24), $\varphi_1^{\mathrm{IT2}}(\boldsymbol{\sigma})$, $\varphi_2^{\mathrm{IT2}}(\boldsymbol{\sigma})$ and $\varphi_3^{\mathrm{IT2}}(\boldsymbol{\sigma})$ are sums of continuous functions $\varphi_{L=3}(\boldsymbol{\sigma})$, $\varphi_{L=6}(\boldsymbol{\sigma})$, $\varphi_{R=3}(\boldsymbol{\sigma})$ and $\varphi_{R=6}(\boldsymbol{\sigma})$. Then, also $\varphi_1^{\mathrm{IT2}}(\boldsymbol{\sigma})$, $\varphi_2^{\mathrm{IT2}}(\boldsymbol{\sigma})$ and $\varphi_3^{\mathrm{IT2}}(\boldsymbol{\sigma})$ are all continuous in the region $[-1,1]^2$, i.e., $\varphi_1^{\mathrm{IT2}} \in \mathcal{C}^0([-1,1]^2) \wedge \varphi_2^{\mathrm{IT2}} \in \mathcal{C}^0([-1,1]^2) \wedge \varphi_3^{\mathrm{IT2}} \in \mathcal{C}^0([-1,1]^2)$. From (24), $\varphi^{\mathrm{IT2}}(\boldsymbol{\sigma})$ is a combination of continuous functions $\varphi_1^{\mathrm{IT2}}(\boldsymbol{\sigma})$, $\varphi_2^{\mathrm{IT2}}(\boldsymbol{\sigma})$ and $\varphi_3^{\mathrm{IT2}}(\boldsymbol{\sigma})$. Therefore, $\varphi^{\mathrm{IT2}}(\boldsymbol{\sigma})$ is also a continuous function in the region $[-1,1]^2$.

□

Theorem 6. *If $\varphi^{\mathrm{IT2}}(\boldsymbol{\sigma})$ indicates FM of DI-IT2-FLC, then $\varphi^{\mathrm{IT2}}(\boldsymbol{\sigma})$ is a monotonic increasing function in the region $[-1,1]^2$ w.r.t. its input variables $\boldsymbol{\sigma}$, i.e., $\frac{\partial \varphi^{\mathrm{IT2}}}{\partial \sigma_1} \geq 0 \wedge \frac{\partial \varphi^{\mathrm{IT2}}}{\partial \sigma_2} \geq 0 \quad \forall \boldsymbol{\sigma} \in [-1,1]^2 \quad \forall \alpha \in [0,1]$.*

Proof. Firstly, let's show that $\varphi(\boldsymbol{\sigma})$ is an increasing function w.r.t. σ_1 $\forall \boldsymbol{\sigma} \in [-1,1]^2$. From 26, $\frac{\partial \varphi_1^{\mathrm{IT2}}}{\partial \sigma_1} = \frac{\alpha(\sigma_2+1)}{(\sigma_1+\sigma_2+\sigma_1\sigma_2-\alpha\sigma_1-\alpha\sigma_2-\alpha\sigma_1\sigma_2+1)^2} \wedge \frac{\partial \varphi_2^{\mathrm{IT2}}}{\partial \sigma_1} = \frac{\alpha\left(\alpha{\sigma_2}^2-{\sigma_2}^2+1\right)}{2(\sigma_1+\alpha+\sigma_1\sigma_2-\alpha\sigma_1-\alpha\sigma_1\sigma_2)^2} + \frac{\alpha\left(\alpha-2\sigma_2-{\sigma_2}^2+2\alpha\sigma_2+\alpha{\sigma_2}^2\right)}{2(\alpha-\sigma_2+\sigma_1\sigma_2+\alpha\sigma_2-\alpha\sigma_1\sigma_2)^2} \wedge \frac{\partial \varphi_3^{\mathrm{IT2}}}{\partial \sigma_1} = \frac{\alpha(1-\sigma_2)}{(\sigma_1\sigma_2-\sigma_2-\sigma_1+\alpha\sigma_1+\alpha\sigma_2-\alpha\sigma_1\sigma_2+1)^2}$. Consequently, $\frac{\partial \varphi_1^{\mathrm{IT2}}}{\partial \sigma_1} \geq 0 \quad \forall \sigma_1 \in [0,1] \quad \forall \sigma_2 \in [0,1] \quad \forall \alpha \in [0,1]$ and $\frac{\partial \varphi_2^{\mathrm{IT2}}}{\partial \sigma_1} \geq 0 \quad (\forall \sigma_1 \in [-1,0] \quad \forall \sigma_2 \in [0,1] \vee \forall \sigma_1 \in [0,1] \quad \forall \sigma_2 \in [-1,0]) \wedge \forall \alpha \in [0,1]$, which is its definition domain, and $\frac{\partial \varphi_3^{\mathrm{IT2}}}{\partial \sigma_1} \geq$

$0 \quad \forall\sigma_1 \in [0,1] \quad \forall\sigma_2 \in [0,1] \quad \forall\alpha \in [0,1]$. Therefore, φ^{T2} is a monotonic increasing in the region $[-1,1]^2$ w.r.t. σ_1. From the first result in Theorem 4, if φ^{T2} is a monotonic increasing in the region $[-1,1]^2$ w.r.t. σ_1, then φ^{T2} is a monotonic increasing in the same region also w.r.t. σ_2. Therefore, φ^{T2} is a monotonic increasing in the region $[-1,1]^2$ w.r.t. both σ_1 and σ_2.

□

4. Simulation Case Study: Control of Spacecraft

Nowadays, considerable attention is given to active control of aerospace systems [48], such as the International Space Station. A typical spacecraft consists of two parts: main rigid body, which contains all the payload instrumentation and control hardware, and mobile attachments, such as solar panels, antennae or telescopes. However, these mobile appendages can induce structural vibrations that in microgravity conditions interfere strongly with the rigid-body attitude dynamics, i.e., angular position θ. This often occurs with moving antennae, e.g., Synthetic Aperture Radars in strip-map mode, and sun-chasing solar panels. Moreover, large solar panels are sensitive to solar radiation pressure, which can induce slight perturbations on the orbit and attitude of the satellite, and Low Earth Orbit satellites with significant cross sections are affected by the atmospheric drag. Therefore, the control of a spacecraft with a mobile attachment is considered to test the controllers developed in Sections 2 and 3.

The spacecraft with a flexible attachment can be modelled with six state variables: angular position θ, angular velocity $\dot{\theta}$, modal coordinate q, modal velocity $\dot{q}$, auxiliary signal z and its derivative $\dot{z}$. Consequently, the system's state is $\begin{bmatrix}\theta & \dot{\theta} & q & \dot{q} & z & \dot{z}\end{bmatrix}^T$. The control input to the system is the torque τ produced by a gyrostat. The model of the system is as in [49]:

$$\begin{cases} \ddot{\theta} &= \tau - 2\omega_n(1-\zeta)\dot{z} \\ \ddot{q} &= (\dot{\theta}^2 - \omega_n^2)q - 2\zeta\omega_n\dot{q} - \alpha(\tau - 2\omega_n(1-\zeta)\ddot{z}) \\ \ddot{z} &= -2\omega_n\ddot{z} - \omega_n^2\dot{z} + \tau, \end{cases} \tag{33}$$

where α is the coupling constant, ω_n is the natural frequency, and ζ is the damping ratio for the flexible appendage.

Remark 8. The parameters of the spacecraft with a flexible arm are selected as in [49], i.e., $\alpha = 0.0802$m, $\omega_n = 22.39$rad/s and $\zeta = 0.001$. Moreover, the control input τ is bounded in the range $[-100, 100]\text{N} \cdot \text{m}$.

4.1. Parameters Settings

Various FOU parameters settings (PSs) are investigated to validate the theoretical analysis. The following PSs are chosen: PS-1: $\alpha = 0.09$, PS-2: $\alpha = 0.25$, PS-3: $\alpha = 0.36$ and PS-4: $\alpha = 0.49$. In addition, a PS with $\alpha = 1.00$ (PS-5) is also tested, which corresponds to DI-T1-FPD according to Remark 5.

4.2. Results

For the simulation case studies, two important problems in control of a spacecraft are considered: reorientation and stabilisation of the spacecraft. During the reorientation of the spacecraft, the attitude of the spacecraft is regulated to reach a new desired value, for example, to increase the signal reception. While the stabilisation of the spacecraft is required after some accident, for example, after the collision with space particles. In both case studies, for the illustrative simplicity, we show only the control of the spacecraft's angular position θ.

Remark 9. In the considered case studies, the maximum position error is πrad, therefore, the proportional input scaling factor is set to: $k_p = \frac{1}{\pi}$; while the maximum angular velocity is 50rad/s, so the derivative input scaling factor is set to: $k_d = \frac{1}{50}$. In addition, the control input is bounded between -100 and 100, therefore, the denormalization gain is set to: $k_o = 100$.

4.2.1. Reorientation of the Spacecraft

In this scenario, the aim of the controller is to change the orientation of the spacecraft. The spacecraft's initial state is $\begin{bmatrix} 0 & 0 & 0 & 0 & 0 & 0 \end{bmatrix}^T$. Then, it has to adjust its angular position from 0rad to πrad.

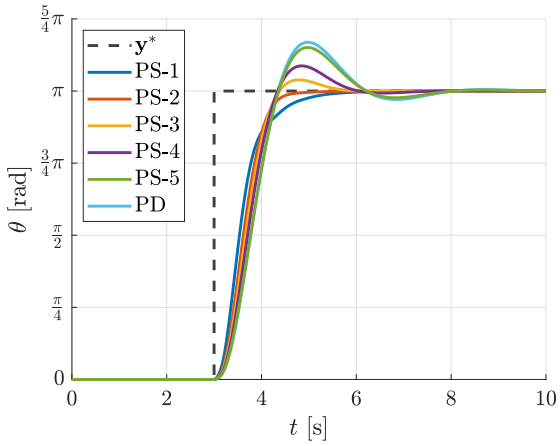

Figure 8: Angular position regulation of the spacecraft by different controllers.

The angular position regulation results of the designed controllers with PS-1, PS-2, PS-3, PS-4 and PS-5 are plotted in Fig. 8. This figure shows that DI-IT2-FPDs with low α (PS-1 and PS-2) have no overshoot, while DI-IT2-FPD with high α (PS-5) has the highest overshoot with relatively slow convergence to the desired value. At the same time, DI-IT2-FPDs with intermediate α (PS-3 and PS-4) combine the aspects of both smooth and aggressive controllers. Therefore, the results of this case study support theoretical claims and expectations.

Table 2 shows the calculated Euclidean mean absolute error (MAE), mean variation of the control signal (MVCS), overshoot, rise time and settling time

Table 2: Properties of developed controllers for attitude control of spacecraft.

Controller	**PS-1**	**PS-2**	**PS-3**	**PS-4**	**PS-5**	**PD**
MAE, [rad]	0.643	0.686	0.711	0.736	0.774	0.779
MVCS, [N · m]	0.008	0.005	0.004	0.003	0.003	0.003
Overshoot, [rad]	~ 0	~ 0	0.122	0.274	0.474	0.532
Rise time, [s]	–	–	2.38	2.34	2.36	2.35
Settling time, [s]	2.22	2.09	2.11	2.15	3.48	3.56

at 10% of the desired value. The Euclidean MAE is computed as

$$\text{MAE} = \frac{1}{S}\sum_{i=1}^{S}|\theta_i - \theta_i^*|, \tag{34}$$

where S is the number of samples, θ_i and θ_i^* are the actual and desired angular positions for the i-th sample, respectively. While MVCS is computed as

$$\text{MVCS} = \frac{1}{S-1}\sum_{i=1}^{S-1}|\tau_{i+1} - \tau_i|, \tag{35}$$

where τ_i is the commanded torque for the i-th sample. As can be observed, DI-IT2-FPD controller with PS-1 results in the lowest MAE value, since an aggressive controller is required to compensate the structural vibrations in microgravity conditions. At the same time, DI-IT2-FPD controllers with PS-4 and PS-5 have the lowest MVCS value which optimises the usage of the satellite's gyrostat. The overshoot is the lowest for DI-IT2-FPD controllers with PS-1 and PS-2 since in frictionless environment an aggressive controller can balance the angular position better. Consequently, the less aggressive controller is, more overshoot it will have.

4.2.2. Stabilisation of the Spacecraft

In this scenario, the aim of the controller is to stabilise the spacecraft. Initially, the spacecraft is spinning around its main axes at -10rad/s, i.e., its initial state is $\begin{bmatrix}\pi & -10 & 0 & 0 & 0 & 0\end{bmatrix}^T$. After 2s the controllers are activated to stop uncontrolled spinning and to stabilise the spacecraft.

The stabilisation results of the designed controllers with PS-1, PS-2, PS-3, PS-4 and PS-5 are plotted in Fig. 9. This figure shows that DI-IT2-FPD with low α (PS-1) has the fastest stabilisation time, while DI-IT2-FPD with high α (PS-5) and PD have the slowest stabilisation time with largest oscillations. At the same time, DI-IT2-FPDs with intermediate α (PS-2, PS-3 and PS-4) combine the aspects of both smooth and aggressive controllers. Therefore, the results of this case study support theoretical claims and expectations.

Table 3 shows the calculated Euclidean MAE, MVCS, overshoot, rise time and settling time at 10% of the desired value. As can be observed, DI-IT2-

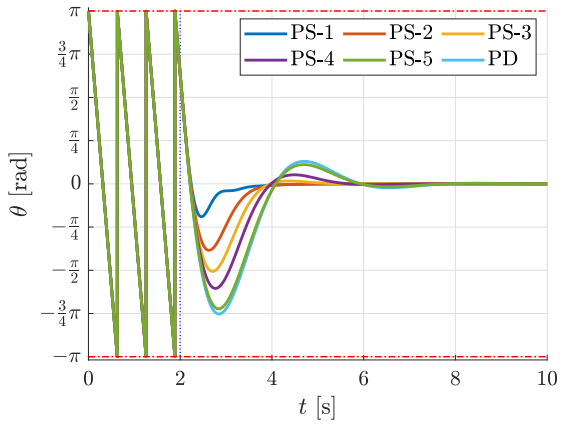

Figure 9: Attitude stabilisation of the spacecraft by different controllers.

FPD controller with PS-1 results in the lowest MAE value, since an aggressive controller is required to compensate the structural vibrations in microgravity conditions. At the same time, DI-IT2-FPD controllers with PS-4 and PS-5 have the lowest MVCS value which optimises the usage of the satellite's gyrostat. The settling time at 10% of the final value is the lowest for the most aggressive controller because it can compensate the structural vibrations fast and avoid the oscillation, while less aggressive controllers are not able to mitigate the oscillations.

5. Experimental Case Study: Control of Unmanned Aerial Vehicle

Nowadays, unmanned aerial vehicles (UAVs) have become a successful cost-effective tool in various applications [50], since they can provide a cheap solution

Table 3: Properties of developed controllers for stabilisation of spacecraft.

Controller	**PS-1**	**PS-2**	**PS-3**	**PS-4**	**PS-5**	**PD**
MAE, [rad]	0.225	0.373	0.497	0.611	0.766	0.801
MVCS, [N · m]	0.009	0.005	0.005	0.004	0.004	0.004
Settling time, [s]	0.703	1.306	1.535	1.695	2.945	3.111

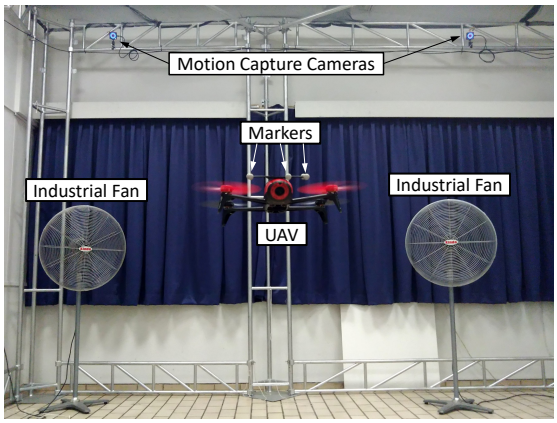

Figure 10: Experimental setup.

to dangerous, dirty and dull missions. However, the design of the flight controllers is still a fundamental problem for multirotors UAVs. Therefore, the real-time control of an aerial robot is considered to test the developed controllers in Sections 2 and 3. Nevertheless, the practical applications of the proposed approach are not limited to this case study.

5.1. Experimental Setup

The experimental flight tests are conducted in the motion capture system, shown in Fig. 10, which provides in real-time the quadcopter's position: x, y and z coordinates. The OptiTrack cameras are able to recognise a particular object according to the pattern of the reflective markers fixed on the object. The cameras provide the estimated position at a rate of 100Hz. Next, the control signal is computed by the ground station (CPU: 2.6GHz, 64bit, quad-core; GPU: 4GB; RAM: 16GB DDR4) and sent to the quadrotor at a rate of 100Hz. The experimental platform is Parrot Bebop 2. To communicate with UAV, the robot operating system (ROS) framework is used.

Remark 10. All developed controllers are implemented in C++ as ROS nodes and are available online at `https://github.com/andriyukr/FLC`.

5.2. Experimental Trajectory

In the experimental scenario, a slanted square-shaped 3D trajectory with 2m square's side, shown in Fig. 11a, is chosen to test different controllers. This trajectory is designed to combine several manoeuvres which include hovering, straight line path, climbing and descending motion. The trajectory includes four way-points, located at $\{[1.0, -1.0, 1.2], [-1.0, -1.0, 0.8], [-1.0, 1.0, 0.8], [1.0, 1.0, 1.2]\}$m. Initially, UAV hovers at $[1, -1, 1.2]$m. Then, it starts flying towards the next way-point located at $[-1.0, -1.0, 0.8]$m where it hovers for 10s before moving to the next way-point.

Remark 11. In the considered case study, PSs are selected to be the same as in Subsection 4.1.

Remark 12. In the considered case study, the maximum position error is 2m, therefore, the proportional input scaling factor is $k_p = \frac{1}{2}$; while the maximum

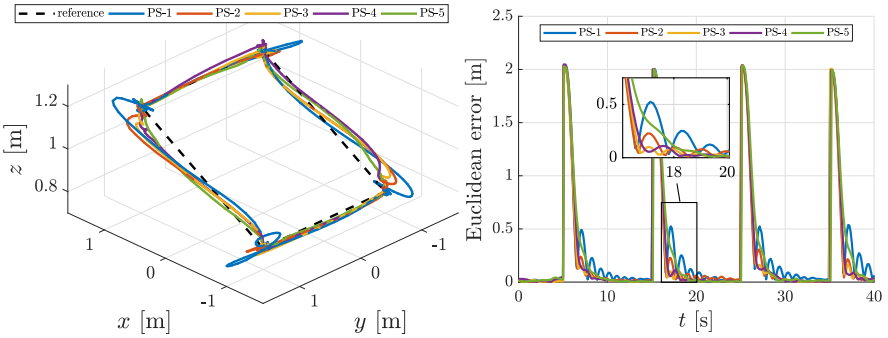

(a) 3D trajectory tracking. (b) Euclidean error.

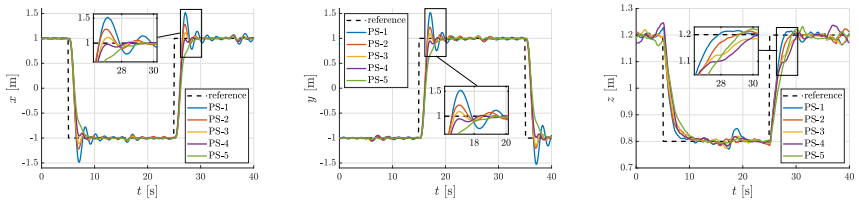

(c) x-axis tracking. (d) y-axis tracking. (e) z-axis tracking.

Figure 11: Trajectory tracking of different DI-IT2-FPD controllers in absence of wind.

speed error is 2m/s, so the derivative input scaling factor is $k_d = \frac{1}{2}$. In addition, the denormalization gain is tuned by trial-and-error method and set to $k_o = 3$.

5.3. Results

The results of 3D trajectory tracking of the designed DI-T1-FPD position controller and DI-IT2-FPD position controllers with PS-1, PS-2, PS-3, PS-4 and PS-5 are plotted in Fig. 11a. The Euclidean error is shown in Fig. 11b for different controllers. The position responses projected on x, y and z axes are shown in Figs. 11c, 11d and 11e. These figures show that DI-IT2-FPD with low α (PS-1) has a high overshoot with an oscillatory action, while DI-IT2-FPD with high α (PS-5) has no overshooting with relatively slow convergence to the desired value. At the same time, DI-IT2-FPDs with intermediate α (PS-2 and PS-3) combine the aspects of both smooth and aggressive controllers. They are fast in converging with low overshoots and small oscillations.

Repeating the experiments of each controller for ten times, Table 4 shows the calculated Euclidean mean absolute error (MAE), mean variation of control signal (MVCS) for x and y axes, mean overshoot, mean rise time and mean settling time at 5% of the desired value. The Euclidean MAE is computed as

$$\text{MAE} = \frac{1}{S}\sum_{i=1}^{S} \|\mathbf{p}_i - \mathbf{p}_i^2\|, \tag{36}$$

where S is the number of samples, $\mathbf{p}_i = \begin{bmatrix} x_i & y_i & z_i \end{bmatrix}^T$ and $\mathbf{p}_i^* = \begin{bmatrix} x_i^* & y_i^* & z_i^* \end{bmatrix}^T$ are the actual and desired positions for the i-th sample, respectively. While

Table 4: Properties of DI-IT2-FPD controllers in absence of wind.

DI-IT2-FPD controller	**PS-1**	**PS-2**	**PS-3**	**PS-4**	**PS-5**
MAE, [m]	0.299	0.241	**0.228**	0.240	0.259
MVCS, [°]	0.314	0.077	0.072	0.041	**0.030**
Overshoot, [m]	0.515	0.230	0.115	0.023	**0.001**
Rise time, [s]	**1.58**	1.60	1.78	3.25	4.63
Settling time, [s]	4.70	2.58	2.13	**2.08**	3.00

MVCS is computed as

$$\text{MVCS} = \frac{1}{S-1}\sum_{i=1}^{S-1}\frac{|\theta^*_{i+1}-\theta^*_i|+|\phi^*_{i+1}-\phi^*_i|}{2}, \tag{37}$$

where θ^*_i and ϕ^*_i are commanded pitch and roll angles of UAV for the i-th sample, respectively. As can be observed from Table 4, DI-IT2-FPD controller with PS-3 results in the lowest MAE value, since this controller has the best combination of aggressiveness, when UAV is far from the desired position, and smoothness, when UAV is close to the desired position. At the same time, DI-IT2-FPD controller with PS-5 has the lowest MVCS value and smallest overshoot, since it generates smooth control commands. On the other hand, DI-IT2-FPD controller with PS-1 has the higher overshoot but the smallest rise time. The settling time at 5% of the final value is the lowest for DI-IT2-FPD controller with PS-4 which undershoots the desired position and is fast to stabilize the UAV.

To check the robustness of the designed controllers, wind disturbances have been introduced. The maximum wind gust is around 5m/s. Table 5 shows the average properties of different DI-IT2-FPD controllers after ten experiments for each case. As can be observed, in the presence of wind the Euclidean MAE increases for all the controllers. However, DI-IT2-FPD controller with PS-3 has a good capability to capture the wind disturbance and it results again in the lowest MAE value. The intensity of control signal again is higher for more aggressive controllers. At the same time, DI-IT2-FPD controller with PS-4 has the smallest overshoot because this controller, similarly to DI-IT2-FPD

Table 5: Properties of DI-IT2-FPD controllers in presence of wind.

DI-IT2-FPD controller	**PS-1**	**PS-2**	**PS-3**	**PS-4**	**PS-5**
MAE, [m]	0.305	0.259	**0.238**	0.250	0.282
MVCS, [°]	0.379	0.105	0.090	0.068	**0.061**
Overshoot, [m]	0.500	0.268	0.120	**0.018**	0.028
Rise time, [s]	**1.60**	1.68	1.70	2.98	4.20
Settling time, [s]	4.88	2.83	2.10	**2.00**	2.78

controller with PS-3, has a good capability to capture the wind disturbance. The rise time increases for more aggressive controllers because the headwind hampers fast flight and the tailwind does not help to fly faster. While the rise time decreases for smoother controllers because the headwind does not reduce the flight speed and the tailwind help to fly faster. For a similar reason, the settling time is larger for aggressive controllers and smaller for smooth controllers.

In addition, DI-T1-FPD and DI-IT2-FPD with PS-3 controllers are compared with the conventional PD controller. The results of 3D trajectory tracking of PD, designed DI-T1-FPD and DI-IT2-FPD with PS-3 position controllers are shown in Fig. 12a. The Euclidean error is shown in Fig. 12b for different controllers. The position (x, y and z) responses are shown in Figs. 12c, 12d and 12e. The experimental video is available at `http://tiny.cc/FM-DI-IT2-FLC`.

For the statistical analysis of control performances, the experiments are repeated ten times for each controller. To compare the trajectory tracking per-

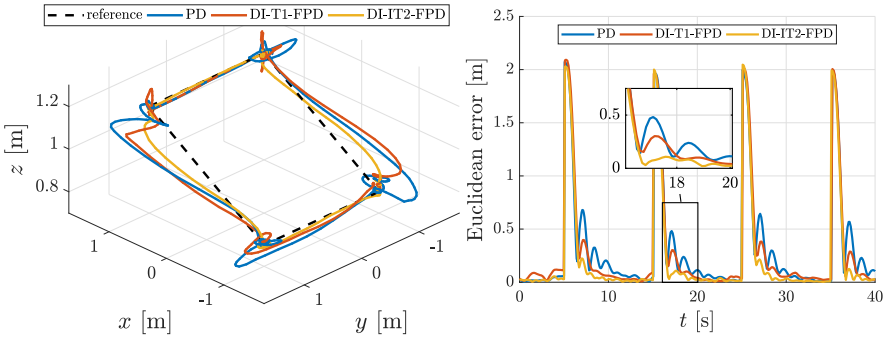

(a) 3D trajectory tracking. (b) Euclidean error.

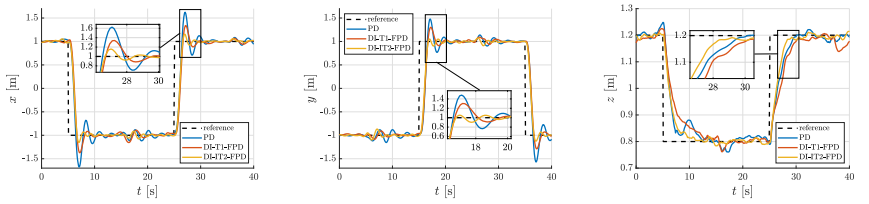

(c) x-axis tracking. (d) y-axis tracking. (e) z-axis tracking.

Figure 12: Trajectory tracking of different position controllers in presence of wind.

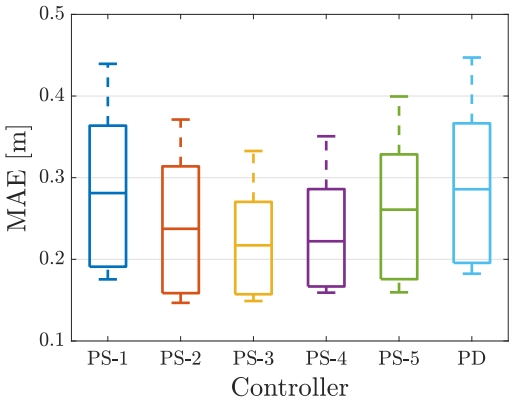

Figure 13: Box-plot of the tracking performances of different controllers in presence of wind.

formances, a box-plot is presented in Figs. 13. It is possible to observe that on average DI-IT2-FPD controller with PS-3 has the lowest MAE and standard deviation on the tested trajectory when compared to other controllers.

Table 6 compares the characteristics of five controllers: standard PD, DI-T1-FPD which uses the standard type-1 fuzzy logic process, DI-T1-FPD* which uses directly FM in (9), DI-IT2-FPD which uses the standard interval type-2 fuzzy logic process and DI-IT2-FPD* which uses directly FM in (24). The average computation time for the traditional DI-T1-FPD and DI-IT2-FPD controllers is larger when compared to that of PD. Since in conventional FLCs, first, the input is fuzzified, then, it goes through the inference engine and, in the end, it is defuzzified. Moreover, in IT2-FLC, the FSs have to be reduced from type-2 to type-1 before the defuzzification. However, in DI-T1-FPD* and DI-IT2-FPD*, a direct FM is used which drastically reduces the computation time. The design, implementation and tuning of PD controllers are easy since it has only two parameters (k_p and k_d). On the other hand, DI-T1-FPD controller has three parameters (k_p, k_d and k_o) and DI-IT2-FPD controller has four parameters (k_p, k_d, k_o and α). Finally, DI-IT2-FPD controller with PS-3 results in the lowest MAE value computed from ten experiments.

5.4. Discussion

From the experimental tests, it can be observed the following:

- For low values of α, DI-IT2-PD controllers generate more aggressive control inputs. Consequently, in a real physical system, it results in more overshoot but lower rising time. If the system is underdamped, it might result in oscillatory behaviour which increases the settling time.

- For high values of α, DI-IT2-PD controllers generate smoother control inputs. Consequently, in a real physical system, it results in undershoot and higher rising time but no oscillations occur. Nevertheless, since the control action is not strong, in disturbed systems, the response will be strongly affected by these disturbances causing more overshoot/undershoot.

- For moderate values of α, DI-IT2-PD controllers combines the characteristics of two cases above.

To summarize, the behaviour of DI-IT2-PD controllers with small values of α, i.e., $0 < \alpha \ll 1$, is more aggressive around the desired position; while, the behaviour of DI-IT2-PD controllers with small values of α, i.e., $0 \ll \alpha \leq 1$, is less aggressive around the desired position. These observations fully confirm the analysis in Subsection 3.2. Therefore, α can be called the *aggressiveness parameter*. Lastly, there is no universally good value of α which can satisfy all

Table 6: Characteristics of different types of controllers.

Controller	**Computation time (average),** [ms]	**Number of parameters**	**MAE with wind** [m]
PD	**0.008**	**2**	0.314
DI-T1-FPD	1.356	3	0.282
DI-T1-FPD*	0.015		
DI-IT2-FPD	1.759	4	**0.238**
DI-IT2-FPD*	0.017		

the cases. The optimal value of α depends on the application, controlled system and working environment.

6. Conclusion and Future Work

In this work, the main focus is to design, deploy and analyse DI-T1-FLC and DI-IT2-FLC with various PSs. First of all, an alternative systematic approach to explicitly derive the mathematical input-output relationships of DI-T1-FLC and DI-IT2-FLC has been presented. These nonlinear closed-form relationships allowed to verify some important characteristics of both DI-T1-FLC and DI-IT2-FLC, like symmetry, continuity and monotonicity. Then, the design method for DI-IT2-FLC has been presented where only one parameter of FOU has to be selected, i.e., aggressiveness parameter α. By only modifying this parameter, DI-IT2-FLC controllers can be designed in an easy manner to have more aggressive or smoother behaviour. In addition, the developed controllers are computationally faster than the traditional FLCs. To prove these theoretical claims, different DI-IT2-FPD controllers with various PSs have been implemented in Matlab and ROS. Then, the developed controllers have been tested, in a simulation case study, for the attitude control of a spacecraft with flexible attachments, and, in an experimental case study, for the way-points tracking control of a quadcopter aircraft. Finally, it has been shown that the theoretical claims and expectations match with the results in the case studies.

In the future, an adaptive controller will be designed to take into account the characteristics of the controlled system and working conditions by adjusting the aggressiveness parameter α. In addition, the presented analysis can be extended to a variety of fuzzy logic systems with Gaussian, Elliptic and other types of MFs. Moreover, the derivation and analysis of FM for triple-input FLCs will be performed by using the presented systematic approach.

Acknowledgment

This research was partially supported by the National Natural Science Foundation of China (No.61806148) and the Fundamental Research Funds for the Central Universities (No. 22120180009). In addition, this research was also partially supported by the Aarhus University, Department of Engineering (28173). The authors are also indebted to Ms. Olena Sarabakha for the technical details of the spacecraft.

References

[1] O. Castillo, L. Amador-Angulo, J. R. Castro, M. Garcia-Valdez, A comparative study of type-1 fuzzy logic systems, interval type-2 fuzzy logic systems and generalized type-2 fuzzy logic systems in control problems, Information Sciences 354 (2016) 257 – 274. doi:10.1016/j.ins.2016.03.026.

[2] L. Cervantes, O. Castillo, Type-2 fuzzy logic aggregation of multiple fuzzy controllers for airplane flight control, Information Sciences 324 (2015) 247 – 256. doi:10.1016/j.ins.2015.06.047.

[3] R.-E. Precup, H. Hellendoorn, A survey on industrial applications of fuzzy control, Computers in Industry 62 (3) (2011) 213 – 226. doi:10.1016/j.compind.2010.10.001.

[4] A. Celikyilmaz, I. B. Turksen, Modeling Uncertainty with Fuzzy Logic: With Recent Theory and Applications, 1st Edition, Springer-Verlag Berlin Heidelberg, 2009. doi:10.1007/978-3-540-89924-2.

[5] T. Kumbasar, H. Hagras, Big Bang–Big Crunch optimization based interval type-2 fuzzy PID cascade controller design strategy, Information Sciences 282 (2014) 277 – 295. doi:10.1016/j.ins.2014.06.005.

[6] C. Fu, A. Sarabakha, E. Kayacan, C. Wagner, R. John, J. M. Garibaldi, Input Uncertainty Sensitivity Enhanced Nonsingleton Fuzzy Logic Controllers for Long-Term Navigation of Quadrotor UAVs, IEEE/ASME Trans-

actions on Mechatronics 23 (2) (2018) 725–734. doi:10.1109/TMECH.2018.2810947.

[7] J. Chen, C. Xu, C. Wu, W. Xu, Adaptive Fuzzy Logic Control of Fuel-Cell-Battery Hybrid Systems for Electric Vehicles, IEEE Transactions on Industrial Informatics 14 (1) (2018) 292–300. doi:10.1109/TII.2016.2618886.

[8] A. Sarabakha, N. Imanberdiyev, E. Kayacan, M. A. Khanesar, H. Hagras, Novel Levenberg–Marquardt Based Learning Algorithm for Unmanned Aerial Vehicles, Information Sciences 417 (2017) 361 – 380. doi:10.1016/j.ins.2017.07.020.

[9] M. Prasad, C. T. Lin, D. L. Li, C. T. Hong, W. P. Ding, J. Y. Chang, Soft-Boosted Self-Constructing Neural Fuzzy Inference Network, IEEE Transactions on Systems, Man, and Cybernetics: Systems 47 (3) (2017) 584–588. doi:10.1109/TSMC.2015.2507139.

[10] K. Tai, A.-R. El-Sayed, M. Biglarbegian, C. I. Gonzalez, O. Castillo, S. Mahmud, Review of Recent Type-2 Fuzzy Controller Applications, Algorithms 9 (2). doi:10.3390/a9020039.

[11] E. Ontiveros, P. Melin, O. Castillo, High order α-planes integration: A new approach to computational cost reduction of General Type-2 Fuzzy Systems, Engineering Applications of Artificial Intelligence 74 (2018) 186 – 197. doi:https://doi.org/10.1016/j.engappai.2018.06.013.

[12] P. Melin, O. Castillo, A review on type-2 fuzzy logic applications in clustering, classification and pattern recognition, Applied Soft Computing 21 (2014) 568 – 577. doi:https://doi.org/10.1016/j.asoc.2014.04.017.

[13] A. K. Ravandi, E. Khanmirza, K. Daneshjou, Hybrid force/position control of robotic arms manipulating in uncertain environments based on adaptive fuzzy sliding mode control, Applied Soft Computing 70 (2018) 864 – 874. doi:https://doi.org/10.1016/j.asoc.2018.05.048.

[14] E. Ontiveros-Robles, P. Melin, O. Castillo, Comparative analysis of noise robustness of type 2 fuzzy logic controllers, Kybernetika 54 (1) (2018) 175–201. doi:10.14736/kyb-2018-1-0175.

[15] E. Kayacan, A. Sarabakha, S. Coupland, R. John, M. A. Khanesar, Type-2 fuzzy elliptic membership functions for modeling uncertainty, Engineering Applications of Artificial Intelligence 70 (2018) 170 – 183. doi:10.1016/j.engappai.2018.02.004.

[16] M. A. Khanesar, E. Kayacan, M. Teshnehlab, O. Kaynak, Analysis of the Noise Reduction Property of Type-2 Fuzzy Logic Systems Using a Novel Type-2 Membership Function, IEEE Transactions on Systems, Man, and Cybernetics, Part B (Cybernetics) 41 (5) (2011) 1395–1406. doi:10.1109/TSMCB.2011.2148173.

[17] D. Wu, J. M. Mendel, Uncertainty measures for interval type-2 fuzzy sets, Information Sciences 177 (23) (2007) 5378 – 5393, including: Mathematics of Uncertainty. doi:10.1016/j.ins.2007.07.012.

[18] D. K. Jana, R. Ghosh, Novel interval type-2 fuzzy logic controller for improving risk assessment model of cyber security, Journal of Information Security and Applications 40 (2018) 173 – 182. doi:10.1016/j.jisa.2018.04.002.

[19] S. Pramanik, D. K. Jana, S. Mondal, M. Maiti, A fixed-charge transportation problem in two-stage supply chain network in gaussian type-2 fuzzy environments, Information Sciences 325 (2015) 190 – 214. doi:10.1016/j.ins.2015.07.012.

[20] O. Castillo, P. Melin, A review on interval type-2 fuzzy logic applications in intelligent control, Information Sciences 279 (2014) 615 – 631. doi:10.1016/j.ins.2014.04.015.

[21] J. M. Mendel, X. Liu, Simplified Interval Type-2 Fuzzy Logic Systems,

IEEE Transactions on Fuzzy Systems 21 (6) (2013) 1056–1069. doi:10.1109/TFUZZ.2013.2241771.

[22] O. Linda, M. Manic, Uncertainty-Robust Design of Interval Type-2 Fuzzy Logic Controller for Delta Parallel Robot, IEEE Transactions on Industrial Informatics 7 (4) (2011) 661–670. doi:10.1109/TII.2011.2166786.

[23] G. K. I. Mann, B.-G. Hu, R. G. Gosine, Analysis of direct action fuzzy PID controller structures, IEEE Transactions on Systems, Man, and Cybernetics, Part B (Cybernetics) 29 (3) (1999) 371–388. doi:10.1109/3477.764871.

[24] H.-X. Li, H. B. Gatland, Conventional fuzzy control and its enhancement, IEEE Transactions on Systems, Man, and Cybernetics, Part B (Cybernetics) 26 (5) (1996) 791–797. doi:10.1109/3477.537321.

[25] H. X. Li, H. B. Gatland, A. W. Green, Fuzzy variable structure control, IEEE Transactions on Systems, Man, and Cybernetics, Part B (Cybernetics) 27 (2) (1997) 306–312. doi:10.1109/3477.558824.

[26] J. Carvajal, G. Chen, H. Ogmen, Fuzzy PID controller: Design, performance evaluation, and stability analysis, Information Sciences 123 (3) (2000) 249 – 270. doi:10.1016/S0020-0255(99)00127-9.

[27] B.-G. Hu, G. K. I. Mann, R. G. Gosine, A systematic study of fuzzy PID controllers-function-based evaluation approach, IEEE Transactions on Fuzzy Systems 9 (5) (2001) 699–712. doi:10.1109/91.963756.

[28] H. Ying, Deriving Analytical Input–Output Relationship for Fuzzy Controllers Using Arbitrary Input Fuzzy Sets and Zadeh Fuzzy AND Operator, IEEE Transactions on Fuzzy Systems 14 (5) (2006) 654–662. doi:10.1109/TFUZZ.2006.877355.

[29] B. Mohan, A. Sinha, Analytical structure and stability analysis of a fuzzy PID controller, Applied Soft Computing 8 (1) (2008) 749 – 758. doi:10.1016/j.asoc.2007.06.003.

[30] T. Kumbasar, H. Hagras, A Self-Tuning zSlices-Based General Type-2 Fuzzy PI Controller, IEEE Transactions on Fuzzy Systems 23 (4) (2015) 991–1013. doi:10.1109/TFUZZ.2014.2336267.

[31] O. Castillo, Design of Stable Type-2 Fuzzy Logic Controllers, Springer Berlin Heidelberg, Berlin, Heidelberg, 2012, Ch. 4, pp. 49–61. doi:10.1007/978-3-642-24663-0_4.

[32] A. Sarabakha, C. Fu, E. Kayacan, T. Kumbasar, Type-2 Fuzzy Logic Controllers Made Even Simpler: From Design to Deployment for UAVs, IEEE Transactions on Industrial Electronics 65 (6) (2018) 5069–5077. doi:10.1109/TIE.2017.2767546.

[33] T. Kumbasar, Robust Stability Analysis and Systematic Design of Single-Input Interval Type-2 Fuzzy Logic Controllers, IEEE Transactions on Fuzzy Systems 24 (3) (2016) 675–694. doi:10.1109/TFUZZ.2015.2471805.

[34] M. Nie, W. W. Tan, Analytical Structure and Characteristics of Symmetric Karnik–Mendel Type-Reduced Interval Type-2 Fuzzy PI and PD Controllers, IEEE Transactions on Fuzzy Systems 20 (3) (2012) 416–430. doi:10.1109/TFUZZ.2011.2174061.

[35] X. Du, H. Ying, Derivation and Analysis of the Analytical Structures of the Interval Type-2 Fuzzy-PI and PD Controllers, IEEE Transactions on Fuzzy Systems 18 (4) (2010) 802–814. doi:10.1109/TFUZZ.2010.2049022.

[36] D. Wu, On the Fundamental Differences Between Interval Type-2 and Type-1 Fuzzy Logic Controllers, IEEE Transactions on Fuzzy Systems 20 (5) (2012) 832–848. doi:10.1109/TFUZZ.2012.2186818.

[37] H. Zhou, H. Ying, A Method for Deriving the Analytical Structure of a Broad Class of Typical Interval Type-2 Mamdani Fuzzy Controllers, IEEE Transactions on Fuzzy Systems 21 (3) (2013) 447–458. doi:10.1109/TFUZZ.2012.2226891.

[38] M. F. Dodurka, T. Kumbasar, A. Sakalli, E. Yesil, Boundary function based Karnik-Mendel type reduction method for Interval Type-2 Fuzzy PID controllers, in: 2014 IEEE International Conference on Fuzzy Systems (FUZZ-IEEE), 2014, pp. 619–625. doi:10.1109/FUZZ-IEEE.2014.6891832.

[39] A. Sakalli, T. Kumbasar, M. F. Dodurka, E. Yesil, The simplest interval type-2 fuzzy PID controller: Structural analysis, in: 2014 IEEE International Conference on Fuzzy Systems (FUZZ-IEEE), 2014, pp. 626–633. doi:10.1109/FUZZ-IEEE.2014.6891830.

[40] H. Zhou, H. Ying, Deriving and Analyzing Analytical Structures of a Class of Typical Interval Type-2 TS Fuzzy Controllers, IEEE Transactions on Cybernetics 47 (9) (2017) 2492–2503. doi:10.1109/TCYB.2016.2570239.

[41] C. M. T. Yip, W. W. Tan, M. Nie, On the difference in control performance of interval type-2 fuzzy PI control system with different FOU shapes, Applied Soft Computing 76 (2019) 517 – 532. doi:https://doi.org/10.1016/j.asoc.2018.12.039.

[42] A. Sarabakha, C. Fu, E. Kayacan, Double-Input Interval Type-2 Fuzzy Logic Controllers: Analysis and Design, in: 2017 IEEE International Conference on Fuzzy Systems (FUZZ-IEEE), 2017, pp. 1–6. doi:10.1109/FUZZ-IEEE.2017.8015485.

[43] D. Wu, J. M. Mendel, On the Continuity of Type-1 and Interval Type-2 Fuzzy Logic Systems, IEEE Transactions on Fuzzy Systems 19 (1) (2011) 179–192. doi:10.1109/TFUZZ.2010.2091962.

[44] W. Pedrycz, F. Gomide, Notions and Concepts of Fuzzy Sets, Wiley-Blackwell, 2007, Ch. 2, pp. 27–44. doi:10.1002/9780470168967.ch2.

[45] J. M. Mendel, Type-1 Fuzzy Systems, Springer International Publishing, Cham, 2017, Ch. 3, pp. 101–159. doi:10.1007/978-3-319-51370-6_3.

[46] J. Mendel, H. Hagras, W.-W. Tan, W. W. Melek, H. Ying, Introduction to Type-2 Fuzzy Logic Control: Theory and Applications, 1st Edition, Wiley-IEEE Press, 2014. doi:10.1002/9781118886540.

[47] N. N. Karnik, J. M. Mendel, Centroid of a type-2 fuzzy set, Information Sciences 132 (1) (2001) 195 – 220. doi:10.1016/S0020-0255(01)00069-X.

[48] A. M. Zanchettin, A. Calloni, M. Lovera, Robust Magnetic Attitude Control of Satellites, IEEE/ASME Transactions on Mechatronics 18 (4) (2013) 1259–1268. doi:10.1109/TMECH.2013.2259843.

[49] M. Reyhanoglu, Slewing maneuver of a flexible spacecraft using finite time control, in: 2008 34th Annual Conference of IEEE Industrial Electronics, 2008, pp. 2667–2671. doi:10.1109/IECON.2008.4758378.

[50] P. A. S. Giacomin, E. M. Hemerly, W. Pedrycz, A probabilistic approach for designing nonlinear optimal robust tracking controllers for unmanned aerial vehicles, Applied Soft Computing 34 (2015) 26 – 38. doi:https://doi.org/10.1016/j.asoc.2015.04.021.